Bulletin of the Geological Survey of Japan, vol. 44(6), p. 377-416, 1993

# Contact metamorphism in andalusite-sillimanite type Tono aureole, Northeast Japan; reactions and phase relations in Fe-rich aluminous metapelites

Yasuko OKUYAMA-KUSUNOSE*

OKUYAMA-KUSUNOSE, Yasuko (1993) Contact metamorphism in andalusite-sillimanite type Tono aureole, Northeast Japan; reactions and phase relation in Fe-rich aluminous metapelites. *Bull. Geol. Surv. Japan*, vol. 44(6) p. 377-416, 12fig., 9 tab., 4pl.

**Abstract**; An extensive thermal aureole develops around Tono granodiorite, the largest mass among Cretaceous I-type granitoids in the Kitakami Mountains, Northeast Japan. The aureole is formed in the surrounding Permo-Carboniferous formations mainly composed of aluminous shale and limestone. The contact metamorphism is low-pressure type (or, andalusite-sillimanite type), and metapelites in the aureole show a systematic progressive change of mineral assemblages in moderately Fe-rich to extremely Fe-rich bulk compositions. Based on the appearance and phase transition of $Al_2SiO_5$ polymorphs, the aureole is divided into three main mineral zones (the paragonite, andalusite and sillimanite zones, with increasing temperatures). Each zone is further subdivided into upper and lower subzones.

In the aluminous metapelites with bulk FeO/(FeO + MgO) ratios of 0.5-0.6, the following isograds are defined by the formation and disappearance of minerals; andalusite-in/paragonite-out, biotite- in, chlorite-out/cordierite-in, muscovite-out/K-feldspar-in, sillimanite-in and garnet-in (in the order of increasing temperatures). Andalusite appears at lower temperatures than the formation of biotite, and is produced by dehydration of paragonite + quartz.

The occurrence of chloritoid is a characteristic feature of the Fe-rich lateritic metapelites ( FeO/(FeO + MgO) > 0.8) in the upper paragonite and the lower andalusite subzones of the Tono aureole. In the presence of muscovite, the chloritoid-bearing assemblages directly forms andalusite and biotite. This paragenetic relation is quite different to the predicted relations in petrogenetic grids derived from thermodynamic calculations. It is also suggested that the andalusite + biotite + chloritoid assemblage is a characteristic assemblage of the typical low-pressure type metapelite distinguished from the low-pressure intermediate type metapelite.

The attempt to estimate conditions of metamorphism from petrogenetic grids derived from thermodynamic calculations had to be abandoned because none of the grids correctly depicted phase relations involving chloritoid. Temperatures in the higher grade zones are estimated by the carbon isotopic geothermometer for limestones intercalating with metapelites. The garnet-biotite geothermometer and garnet-$Al_2SiO_5$-plagioclase-quartz geobarometer are also applied to garnet-bearing high-grade samples. The estimated temperatures are lower than 490°C in the paragonite zone, 490°C to 600°C in the andalusite

* Geological Museum

Keywords: Phase relation, contact metamorphism, metapelite, andalusite-sillimanite metamorphism paragonite, chloritoid., Tono, Kitakami

zone, 600°C to 670°C in the lower sillimanite subzone, and 670°C to 720°C in the upper sillimanite subzone.

The carbon isotopic temperature combined with $Al_2SiO_5$ equilibrium of Holdaway (1971) gives a total pressure of 2.3 kbar at the andalusite-sillimanite transition. Assuming a pressure of 2.3 kbar, the carbon isotopic temperature at the muscovite + quartz dehydration indicates that this reaction occurred at a temperature lower than that of $P_{H2O} = P_{total}$ by an extensive dilution of metamorphic fluid by $CH_4$ and/or $CO_2$. The estimated temperatures, pressures and compositions of metamorphic fluid suggest that the actual position of And-Sil equilibrium is better approximated by Holdaway (1971) than by Pattison (1989).

## 1. Introduction

Phase relations of metapelites in the contact aureole may provide an important clue on the level of emplacement of an igneous pluton that produced the aureoles. As is shown in the recent review by Pattison and Tracy (1991), there are several types, or facies series, of contact metamorphic phase relations which may be caused by the difference in prevailed pressures.

By the accumulation of thermodynamic data on minerals, it is now possible to construct a petrogenetic grid through thermodynamic calculation. The grids recently proposed by Spear and Cheney (1989), Powell and Holland (1990), Wang and Spear (1991) and Dymoke and Sandiford (1992) rather successfully describe isograd sequence for medium-pressure type metamorphism. However, the low-pressure phase relations in these grids are mutually inconsistent and do not agree with natural pelitic phase relations. The major discrepancy in these grids lies in the stability relations of Fe-Al silicates (garnet, staurolite and chloritoid) to andalusite, cordierite and chlorite in the low-pressure region below the triple point of $Al_2SiO_5$. The failures in thermodynamic prediction demands phase petrologic study of natural low-pressure metapelites, including those in the contact aureole.

This paper deals with progressive metamorphism in the contact aureole around the Tono granodiorite mass, Kitakami Mountains, Northeast Japan. The contact metamorphism is andalusite-sillimanite type (or, low-pressure type of Miyashiro, 1961), and is known by the occurrence of chloritoid in the low-grade zone since Seki (1954, 1957) who first gave detailed description of metapelitic rocks of this area. The chloritoid has been considered to be retrogressive (Seki, 1954), however, Okuyama (1980) has revealed that the chloritoid in the low-grade zone is progressively formed by a reaction between Fe-chlorite and pyrophyllite. This paper describes stable assemblages involving chloritoid, and discusses their importance as diagnostics of typical andalusite-sillimanite type metamorphism.

## 2. Geological setting

The Tono granodiorite is the largest pluton among the Cretaceous I-type granitoids in the Kitakami Mountains (Kanisawa and Katada, 1989). The mass is mainly composed of biotite- and hornblende-bearing granodiorite to tonalite, and is associated with small gabbroic stocks (Kanisawa *et al.*, 1986; Kanisawa and Ishikawa, 1987). Biotite K-Ar ages from granodiorite are 110-122 Ma (Kawano and Ueda, 1965).

Geologic map in the central portion of the South Kitakami Mountains is compiled by Ehiro (1989). The country rock that was intruded and thermally metamorphosed by the Tono mass is epicontinental sediments of Paleozoic era (Fig. 1). The country rock mainly comprises intercalating beds of normal clastic sediments and abundant limestone of Early Carboniferous to Middle Permian period (Saito and Hashimoto, 1982; Kawamura and Kawamura, 1989). The Carboniferous formations in the southern part of the aureole also interbeds a fairly large amount of andesitic volcanic rocks. Siluro - Devonian sediments also crop out in restricted areas in the south-

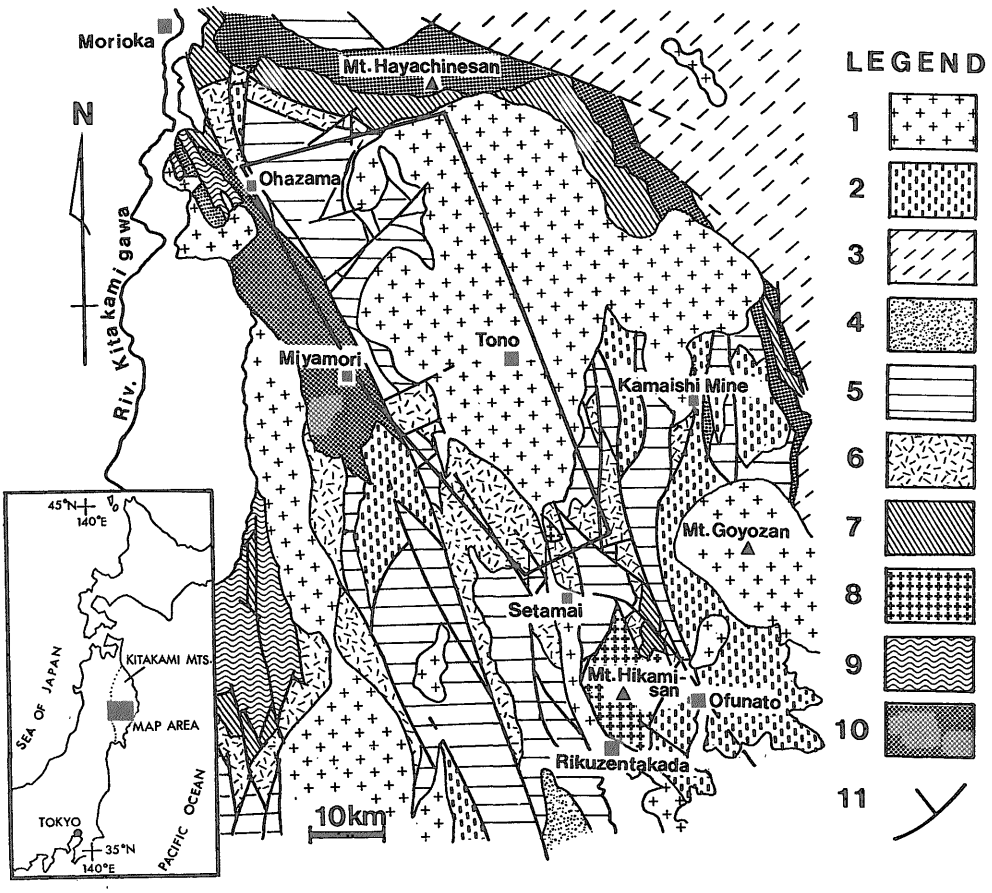


Fig. 1 Outline of geology in the central part of the Kitakami Mountains (modified from Ehiro, 1989). Legend: 1; Cretaceous granitic rocks and related igneous plutons, 2; Cretaceous volcanic rocks, 3; Mesozoic and Paleozoic strata in the Northern Kitakami Mountains, 4; Trias System, 5; Permian System, 6; Carboniferous System, 7; Siluro-Devonian System, 8; Hikami granite mass and related older granite, 9; Motai and Unoki metamorphic rocks, 10; mafic and ultramafic rocks of Miyamori and Hayachine complexes, 11; faults. The study area shown in Fig. 2 are the enclosed area in the central part of this figure.

ern part of the aureole (Kawamura, 1985a). In the western margin of the aureole, the Paleozoic sediments are further intruded by the ophiolitic Miyamori ultramafic complex (Ozawa, 1984, 1988). The mass was emplaced along the Hizume-Kesennuma transcurrent fault (Ehiro, 1977), and is weakly metamorphosed in its eastern margin (Ozawa *et al.*, 1988).

The pelitic metamorphic rocks in the Tono aureole are characterized by the occurrence of peculiar rock type with lateritic compositions. This type of rocks contains chloritoid-bearing assemblages in the low-grade metamorphism. Kawamura *et al.* (1985) reported an intimate association of lateritic shales with limestone beds of the Odaira Formation in the Setamai area, south of the Tono mass. Furthermore, Kawamura (1985a, b) reported that the lateritic shale is present in the basal part of the Permian Sakamotozawa Formation and its equivalents. The sedimentary rocks of these horizons also crop out in the Tono aureole

(Plate I-a), frequently repeated by folds and faults. By the rather common occurrence of lateritic metapelites, the Tono contact metamorphic aureole becomes a suitable field to study phase relations in Fe-rich portion of the pelitic system.

## 3. Mineral zones and petrography

The Paleozoic shale around the aureole of Tono mass is characteristic in its generally high $Al_2O_3$ content, low alkaline contents, low MnO content and low MgO/FeO and $K_2O$/$Na_2O$ ratios (Katada and Ono, 1968). The metapelites of the Tono aureole also show similar characteristics in bulk compositions. Table 1 shows averaged chemical compositions of aluminous metapelites, the common type of pelitic rocks in the aureole, and lateritic metapelites. The pelitic compositions fall in the Al-rich portion of the chlorite-muscovite join in the $Al_2O_3$-$K_2O$-FeO-MgO tetrahedron. Another characteristic to be noted is low MnO contents of metapelites. This results in the low Mn content in chlorite in the low-grade zone, and low spessartine content in garnet in the high-grade zone.

The metapelites of the Tono aureole widely develop andalusite and sillimanite in the medium to high grade zones because of their aluminous bulk compositions. The aureole is divided into three main mineral zones by the formation and phase transition of $Al_2SiO_5$ minerals (Figs. 2, 3). The lowest grade zone which was called chlorite zone in the previous papers (Okuyama, 1980; Okuyama-Kusunose, 1985; Okuyama-Kusunose and Itaya, 1987) is renamed as paragonite zone in this paper because of the presence of paragonite in this zone. The presence of paragonite leads to the formation of andalusite well below the temperature of decomposition of muscovite with quartz. Each zone is further subdivided into the upper and lower subzones based on the paragenetic changes of Fe-Mg silicates in metapelites containing quartz, muscovite (or K-feldspar, above the decomposition of muscovite + quartz), graphite (or, carbonaceous matter, in low-grade zone), a Ti-phase (sphene or ilmenite) and Fe sulfide(s) (pyrite and/or pyrrhotite). The paragenetic relations in the aluminous metapelite and in the lateritic metapelite are systematically different, except in the highest grade zone. In the subsequent sections, mineral abbreviations follow Kretz (1983).

Table 1 Averaged composition of aluminous and lateritic metapelites. Source data are listed in Okuyama-Kusunose (1988). The compositions excluding $H_2O$ and ignition losses are at first normalized to 100%, and then averaged. All the Fe oxides are recalculated to FeO (shown as $FeO_t$ in the Table).

| Rock type | Aluminous metapelites | Lateritic metapelites |
|---|---|---|
| No. of analysis | 26 | 11 |
| $SiO_2$ | 64.06(4.07) | 59.74(7.81) |
| $TiO_2$ | 1.11(0.21) | 1.22(0.38) |
| $Al_2O_3$ | 20.70(2.61) | 23.44(4.60) |
| $FeO_t$ | 6.65(1.75) | 12.15(3.58) |
| MnO | 0.05(0.03) | 0.08(0.07) |
| MgO | 2.95(0.63) | 1.04(0.48) |
| CaO | 0.57(0.33) | 0.55(0.50) |
| $Na_2O$ | 2.11(0.80) | 0.90(0.65) |
| $K_2O$ | 1.73(0.71) | 0.85(0.41) |
| $P_2O_5$ | 0.07(0.05) | 0.03(0.02) |
| Total | 100.00 | 100.00 |
| FeO/(FeO+MgO) | 0.560 | 0.868 |

### 3.1 Paragonite zone and its lower and upper subzones

Metapelites of the paragonite zone commonly contain paragonite (Pg) with chlorite (Chl) and muscovite (Ms). The characteristic assemblage is (A1) Pg + Chl (+ albite) in the aluminous metapelite. This assemblage is stable in the aluminous metapelite throughout the paragonite zone. In the lateritic metapelite, pyrophyllite (Prl) also occurs stably with chlorite, muscovite and paragonite (the assemblage L1; Pg + Prl + Chl). Pyrophyllite does not coexist with albite and/or calcite.

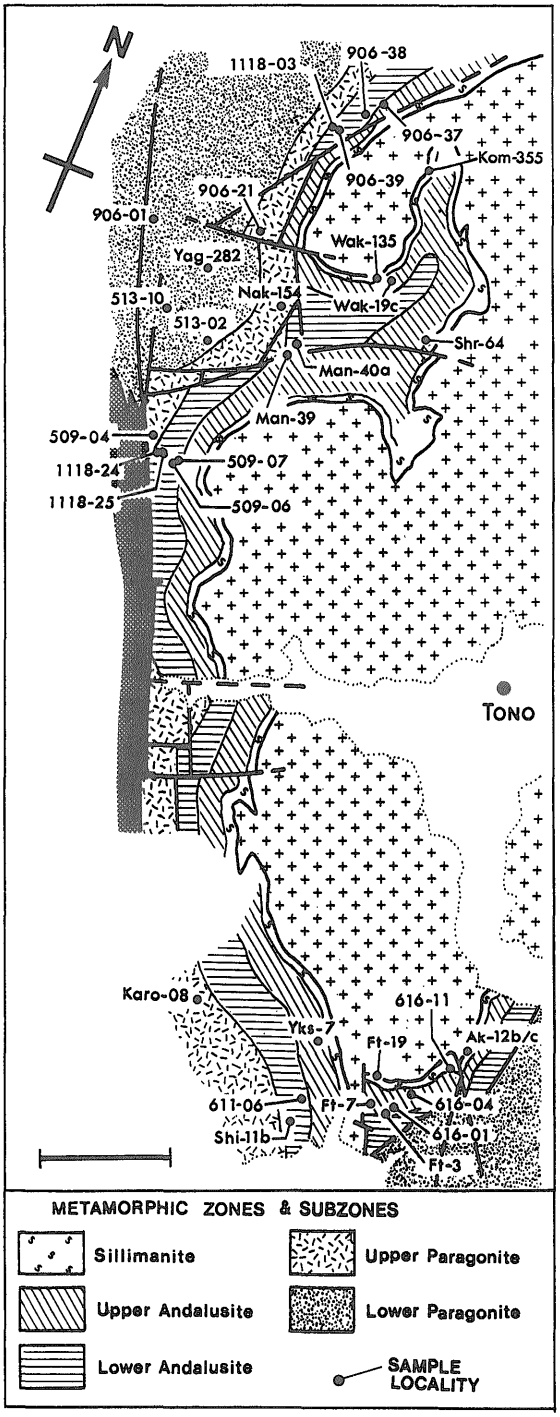


Fig. 2 Progressive zones of contact metamorphism in the aureole around the Tono granodiorite mass. The locations of samples discussed in the text are also shown.

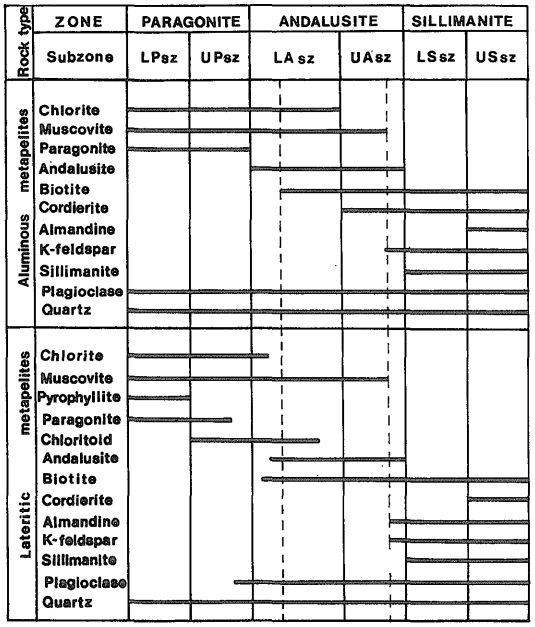


Fig. 3 Stability relation of minerals in the Tono contact aureole.

With increasing temperatures, pyrophyllite in the lateritic metapelite reacts with Fe-chlorite to form chloritoid (Okuyama, 1980). The reaction defines the onset of upper paragonite subzone (Fig. 3). The mineral assemblage in this type of pelitic rock changes from (L1) in the lower subzone to (L2) Pg + Chl + Cld. Margarite also occurs sporadically in this subzone coexisting with chlorite, chloritoid, paragonite and zoisite in slightly calcic metapelites (Okuyama-Kusunose, 1985). Plagioclase is also absent in the lateritic metapelite with the assemblages (L2). In the uppermost portion of the paragonite zone, however, paragonite disappears from the lateritic metapelite and Chl + Cld begins to coexist with oligoclase (the assemblage L3; Chl + Cld, with Pl). The change occurs a few hundred meters to the downgrade side of the andalusite isograd.

The metapelite of the lower paragonite subzone is fine-grained slate with distinct cleavage. Under the microscope, the metapelite exhibits a texture that dark-colored, subparallel streaks are sandwiching lensoid aggregates of chlorite and white micas (Plate II-a).

The dark-colored streak, or dusty part (Oho, 1981), concentrates carbonaceous material and very fine-grained phyllosilicates. Fine-grained polygonal quartz, albite and calcite are present mainly in the matrix and lensoid part. Euhedral pyrite and anhedral sphene occur commonly as accessory phases. The increasing temperatures in the paragonite zone promote grain growth of minerals in metapelites. In most cases, the metapelites become less cleavable in the upper paragonite subzone due to grain growth of quartz and albite (Plate II-b). Conversely, micaceous metapelite frequently becomes schistose due to distinct grain growth of micas and chlorite. Chloritoid of this subzone forms small, tabular porphyroblasts or rosettes of radiating crystals (Plate II-c).

The paragonite zone extends more than 7 km away from the Tono granodiorite mass (Fig. 2). In the northern part, the western margin of aureole is limited by the intrusion of Miyamori ultramafic complex. In the southern part of the aureole, spotted slate containing chloritoid and/or andalusite is sporadically found more than 10 km away from the Tono mass. The random distribution of spotted slates suggests that the thermal structure in this area is rather complicated, probably due to concealed bodies of small granitic mass.

### 3.2 Lower andalusite subzone

The onset of andalusite zone is marked by the appearance of andalusite (And) with disappearance of paragonite in the aluminous metapelite (Fig. 3). The andalusite isograd passes about 1.9 to 2.3 km away from the Tono mass (Fig. 2). Andalusite forms minute prisms, with a length less than 0.1 mm, in massive hornfels. In some of the micaceous metapelite, andalusite forms large idioblasts up to 5 cm in length scattering in the matrix. In both cases, andalusite is chiastolitic with cross-like arrangement of dust inclusions (Plate II-d).

Andalusite initially coexists only with chlorite, muscovite, oligoclase and quartz (the assemblage A2; And + Chl). Biotite (Bt) appears about 50 to 100 meters to the upgrade side of the andalusite isograd, and the assemblage changes from (A2) to (A3) And + Bt + Chl. This assemblage is stable throughout the remaining part of lower andalusite subzone. The modal proportions of andalusite and biotite increase whereas those of chlorite and muscovite decrease toward high temperatures.

In the lateritic metapelite, the assemblage (L3) still occurs stably near the andalusite isograd. Chloritoid in some of the lateritic metapelite grows up to be large idioblasts up to 1 cm in diameter (Plate I-b). Characteristic hourglass structure is observed commonly in the large chloritoid prisms (Plate III-a). The assemblage (L3) is limited to a narrow area, and is replaced by a biotite-bearing assemblage of (L4) Bt + Chl + Cld. Although the coexistence of chloritoid and biotite is relatively rare (Deer et al., 1982), this assemblage occurs commonly in the lower andalusite subzone of the Tono aureole. Andalusite also occurs occasionally with biotite in the lateritic metapelite, forming an assemblage (L4') Bt + Chl + Cld + And. Field occurrence suggests that biotite is formed at slightly lower temperatures in the lateritic metapelite than in the aluminous metapelite. At the locality of sample Shi-11b containing the assemblage (L4) (Fig. 2), the intercalating alumi-nous metapelite does not carry biotite.

Further to the upgrade side, chlorite disappears from the lateritic metapelite and the assemblage changes to (L5) And + Bt + Cld (Plate III-b). With a further increase in temperature, the modal proportion of andalusite and biotite increases rapidly in this assemblage. This leads to the disappearance of chloritoid from the lateritic metapelite containing muscovite, oligoclase and quartz (the assemblage L6; And + Bt). Chloritoid, however, occasionally remains in the lateritic metapelite. Because muscovite is modally smaller than chloritoid in most of the lateritic metapelites, it is consumed up in the reaction with chloritoid. The disappearance of muscovite in the middle grade conditions leads to the formation of a variety of muscovite-

absent assemblages. The garnet- and ortho-amphibole-bearing assemblages are described by Seki(1957) from the middle-grade portion of the Tono aureole where andalusite is a stable form of the $Al_2SiO_5$ polymorphs. The assemblages, however, are stable only in the absence of muscovite.

### 3.3 Upper andalusite subzone

The onset of the upper andalusite subzone is marked by the appearance of cordierite (Crd) with disappearance of chlorite in the aluminous metapelite (Fig. 3). The assemblage change from (A3) to (A4) And + Bt + Crd (+ Ms). Cordierite initially forms small ovoid spots relatively poor in silicate inclusions (Plate III-c). With increasing temperature, the fine-grained matrix of the pelitic hornfels gradually becomes coarse-grained. However, the preferred orientation of micas is still remaining in most cases.

In the uppermost part of the andalusite subzone about 150-200m to the downgrade side of the sillimanite isograd, muscovite decomposes into K-feldspar (Kfs) and andalusite by a reaction with quartz (the assemblage A5; And + Bt + Crd, with Kfs) (Fig. 3). Cordierite in K-feldspar-bearing hornfels be-comes irregularly shaped and contains abundant inclusions of quartz and micas (Plate III-d). The margin of coexisting andalusite also becomes poikiloblastic with abundant quartz inclusions.

The paragenetic change in the lateritic metapelite is less clear due to limited occurrence of this rock type in the upper andalusite subzone. Pelitic hornfels with the And + Bt assemblage occurs sporadically in this subzone where the assemblage (A4) occurs widely in common aluminous metapelites. Some of the biotite in the assemblage (L6) is extremely Fe-rich with $X_{Fe}$ (= Fe/Fe+Mg) as high as 0.83 (see next section). It is not clear from the field occurrence whether andalusite and Fe-biotite stably coexist with K-feldspar. In the upper andalusite subzone where K-feldspar becomes stable, garnet first appears in pelitic hornfels with bulk composition similar to the lateritic metapelite of the lower grade zones. Garnet is as small as 0.2mm and is widely dispersed in the matrix with abundant biotite (Plate IV-a). Garnet is rich in almandine molecule. The assemblage is (L7) Alm + And + Bt (+ Kfs). Note that cordierite does not appear in the lateritic metapelite of the upper andalusite subzone.

### 3.4 Lower sillimanite subzone

In the high-grade part of the aureole about 100 to 200 m away from the Tono mass, sillimanite (Sil) appears in pelitic hornfels con-taining quartz, plagioclase and K-feldspar (the assemblage A6; Sil + Bt + Crd) (Fig. 3). Sillimanite usually occurs as an aggregate of fibrous crystals surrounding a short prism of andalusite and rounded cordierite (Plate IV-b). It also occurs as elongated prisms with distinct (001) parting (Plate IV-c). The thickness of sillimanite crystals normal to c-axis is ranging from 5 $\mu$m to 50 $\mu$m. Although some of the values of crystal thickness are crossing the sillimanite/"fibrolite" boundary defined by Kerrick and Speer (1988), the mineral is treated as single-phase sillimanite in this study. The modal abundance of sillimanite tends to increase toward the high-temperature side with a modal decrease of andalusite. The mode of occurrence of these two alumino-silimates suggests that sillimanite is produced from andalusite by a sluggish phase transition. Kerrick (1987) discussed an intimate association of fibrous sillimanite with biotite to be a characteristic of thermal aureole. The association of these two minerals, however, is quite rare in the Tono contact metamorphic aureole.

In the sillimanite-bearing metapelite, the modal abundance of cordierite and K-feldspar increase with increasing temperatures while that of biotite decreases gradually. This suggests a prograde reaction of biotite and sillimanite to produce cordierite and K-feldspar, although the direct textural evidence, such as the sillimanite inclusion in cordierite (e.g., Bluemel and Schreyer, 1977), has not been observed.

### 3.5 Upper sillimanite subzone

Further to the upgrade side, almandine garnet appears commonly coexisting with cordierite, biotite, K-feldspar and quartz (the assemblage A7; Alm + Bt + Crd, Plate IV-d). This pelitic assemblage occurs in a few tens of meters of the very contact with Tono mass. Sillimanite is rather rare in pelitic rocks of this subzone, although this subzone is called the upper sillimanite subzone. Sillimanite occurs only in the assemblage (A7') Alm + Bt + Crd + Sil (+ Kfs). Biotite in this assemblage usually occurs forming a decussate aggregate partially replacing garnet. The texture suggests that this biotite is formed by partial resorption of garnet in the later stage. Almandine garnet forms idioblasts of various sizes (Plate IV-d). The modal abundance of garnet is quite variable. Some of the pelitic hornfels with assemblage (A7) contains garnet more than 10 modal percent. The bulk $Al_2O_3$ and FeO contents are quite similar to the chloritoid-bearing metapelites in the low-grade zone This suggests that the assemblage (A7) is stably formed not only in the aluminous metapelite but also in the lateritic metapelite.

The garnet-cordierite rocks frequently undergo partial melting in the highest-grade portion of low-pressure type metamorphism (e.g., Gil Ibaruguchi and Martinez, 1982; Evans and Speer, 1984; Montel *et al.*, 1992). The metapelitic rocks of the upper sillimanite subzone of the Tono aureole, however, do not show textures of partial melting.

## 4. Mineral chemistry

Minerals in pelitic rocks were analyzed by use of an X-ray analyzing system at Tohoku University. The system is composed of Hitachi scanning electron microscope S-560 and Kevex energy dispersive X-ray detector. The analytical procedure follows Fujimaki and Aoki (1985). X-ray count time was set to be more than 500 seconds to analyze some minor elements. Fe in Fe-Mg silicates and muscovite is assumed to be $Fe^{2+}$. Fe in aluminosilicate phases is also assumed to be $Fe^{3+}$. Chloritoid, cordierite and garnet are more or less zoned. The rim compositions of mineral grains that are not resorbed or altered are chosen to represent equilibrium compositions in each sample. The location of analyzed samples are shown in Fig. 2.

### 4.1 Chlorite

Chemical composition of chlorites in the study area covers a wide range in $X_{Fe}$ (Table 2). The chlorites is relatively aluminous as compared to that in the chlorite-muscovite assemblage of some regional terranes of intermediate- and low-pressure metamorphism (Laird, 1988). Chlorite in the Pg + Chl and Prl + Pg + Chl assemblages becomes slightly silicic with decreasing $X_{Fe}$. In chlorite with a similar $X_{Fe}$, Al and Si contents of chlorite are comparable in the Pg + Chl and And + Chl assemblages. This suggests that there is a negligible effect of metamorphic temperature on chlorite compositions. Mn contents are notably low and $X_{Mn}$ (= Mn / Fe + Mg + Mn) ratios are mostly less than 0.01. This value is distinctly lower than that for chlorite in common metapelitic rocks (cf. Symmes and Ferry, 1992, assuming $X_{Mn}$ = 0.02-0.05, in chlorite of chlorite-muscovite assemblage).

### 4.2 Chloritoid

Chloritoid is generally poor in Mg and Mn as shown in Table 3. The amount of Mn-chloritoid component, $MnAl_2SiO_5(OH)_2$, is mostly less than $X_{Mn}$ = 0.01. Chloritoid in the upper paragonite subzone is slightly zoned with increasing Mg content toward rim. Chloritoid of the lower andalusite subzone sometimes shows complex chemical zoning, with Mg maximum in the mantle.

### 4.3 Cordierite

Cordierite contains minor amounts of Mn, Na and Ca (Table 4). Cordierite in the garnet-free assemblages tends to concentrate Mn as compared to that coexisting with garnet. There is a weak correlation between Na content and excess Al in the tetrahedral site ($^{IV}$Al-1, at O = 18) (Fig. 4). This suggests that Na, probably in the channel site (Goldman *et*

Table 2 Microprobe analyses of chlorite.

| | Lower paragonite subzone | | | | Upper paragonite subzone | | | | | | | Lower andalusite subzone | | |
|---|---|---|---|---|---|---|---|---|---|---|---|---|---|---|
| Sample | 906-01 | 513-10 | 513-02 | Yag-282 | Karo-26 | 906-21 | Nak-154 | 509-04 | Karo-08 | 514-01 | 509-05 | 611-03 | 1118-03 | 1118-24 |
| Assemblage | A1 | A1 | A1 | L1 | A1 | A1 | A1 | L2 | L2 | C | C | A2 | A2 | L3 |
| $SiO_2$ | 23.53 | 23.26 | 23.89 | 22.74 | 23.21 | 25.84 | 23.05 | 23.42 | 23.01 | 23.90 | 23.44 | 23.55 | 24.00 | 22.48 |
| $Al_2O_3$ | 23.88 | 23.40 | 25.33 | 25.65 | 24.19 | 24307 | 23.29 | 26.06 | 25.67 | 24.01 | 25.11 | 23.91 | 23.93 | 24.09 |
| FeO | 33.56 | 30.45 | 29.15 | 35.64 | 30.77 | 26.62 | 31.30 | 32.76 | 33.46 | 30.76 | 32.05 | 30.68 | 29.25 | 37.42 |
| MnO | 0.11 | 0.17 | 0.89 | 0.20 | 0.56 | 0.27 | 0.11 | 0.24 | 0.08 | 0.08 | 0.10 | 0.22 | 0.34 | 0.10 |
| MgO | 7.76 | 9.40 | 9.83 | 5.12 | 8.64 | 11.83 | 8.55 | 6.63 | 6.73 | 9.98 | 6.15 | 9.25 | 10.06 | 4.59 |
| Total | 88.84 | 86.68 | 89.09 | 89.35 | 87.37 | 88.86 | 86.30 | 89.11 | 88.95 | 88.79 | 86.85 | 87.61 | 87.58 | 88.68 |
| | Numbers of cations on the basis of 28 oxygens | | | | | | | | | | | | | |
| Si | 5.107 | 5.112 | 5.054 | 4.957 | 5.071 | 5.369 | 5.110 | 5.029 | 4.976 | 5.112 | 5.155 | 5.112 | 5.167 | 5.005 |
| $^{IV}Al$ | 2.893 | 2.888 | 2.946 | 3.043 | 2.929 | 2.631 | 2.890 | 2.971 | 3.024 | 2.888 | 2.845 | 2.888 | 2.833 | 2.995 |
| $^{VI}Al$ | 3.216 | 3.165 | 3.371 | 3.548 | 3.291 | 3.319 | 3.197 | 3.624 | 3.518 | 3.177 | 3.663 | 3.228 | 3.240 | 3.326 |
| Fe | 6.092 | 5.589 | 5.158 | 6.498 | 5.614 | 4.625 | 5.804 | 5.883 | 6.051 | 5.494 | 5.894 | 5.569 | 5.267 | 6.967 |
| Mn | 0.020 | 0.032 | 0.159 | 0.037 | 0.103 | 0.048 | 0.021 | 0.044 | 0.015 | 0.014 | 0.019 | 0.040 | 0.062 | 0.019 |
| Mg | 2.511 | 3.075 | 3.100 | 1.664 | 2.810 | 3.664 | 2.826 | 2.122 | 2.169 | 3.179 | 2.016 | 2.992 | 3.229 | 1.523 |
| Total | 19.839 | 19.861 | 19.788 | 19.747 | 19.818 | 19.656 | 19.847 | 19.673 | 19.753 | 19.859 | 19.592 | 19.825 | 19.797 | 19.835 |
| $X_{Fe}$ | 0.708 | 0.645 | 0.625 | 0.796 | 0.666 | 0.558 | 0.673 | 0.735 | 0.736 | 0.745 | | 0.651 | 0.620 | 0.821 |

Table 2 (Continued)

| Sample | Man−39 | Man-40a | Man-40b | 906-39 | 611-04 | 611-06 | 906-38 | 1118-25 | Shi-11b | 509-06 |
|---|---|---|---|---|---|---|---|---|---|---|
| | Lower andalusite subzone (continued) | | | | | | | | | |
| Assemblage | A3 | A3 | A2 | A3 | A3 | A3 | A3 | L4 | L4 | L4 |
| $SiO_2$ | 24.01 | 24.29 | 25.61 | 24.73 | 24.84 | 24.97 | 25.16 | 22.22 | 22.08 | 22.48 |
| $Al_2O_3$ | 23.24 | 23.88 | 22.86 | 23.30 | 23.08 | 22.68 | 22.86 | 24.60 | 24.62 | 24.91 |
| FeO | 28.65 | 27.82 | 25.52 | 27.42 | 26.17 | 25.88 | 25.82 | 36.87 | 36.47 | 34.39 |
| MnO | 0.47 | 0.31 | 0.44 | 0.23 | 0.26 | 0.38 | 0.22 | 0.06 | 0.06 | 0.08 |
| MgO | 10.58 | 10.75 | 12.18 | 11.29 | 12.03 | 12.45 | 12.79 | 4.98 | 5.21 | 6.30 |
| Total | 86.95 | 87.05 | 86.61 | 86.97 | 86.38 | 86.36 | 86.85 | 88.73 | 88.44 | 88.16 |
| | Numbers of cations on the basis of 28 oxygens | | | | | | | | | |
| Si | 5.202 | 5.217 | 5.458 | 5.301 | 5.333 | 5.360 | 5.354 | 4.933 | 4.911 | 4.925 |
| $^{IV}Al$ | 2.798 | 2.783 | 2.542 | 2.699 | 2.667 | 2.640 | 2.646 | 3.067 | 3.089 | 3.075 |
| $^{VI}Al$ | 3.137 | 3.263 | 3.192 | 3.189 | 3.164 | 3.140 | 3.088 | 3.361 | 3.356 | 3.348 |
| Fe | 5.191 | 4.998 | 4.542 | 4.916 | 4.692 | 4.639 | 4.595 | 6.836 | 6.775 | 6.291 |
| Mn | 0.086 | 0.056 | 0.079 | 0.042 | 0.048 | 0.069 | 0.040 | 0.011 | 0.011 | 0.014 |
| Mg | 3.417 | 3.442 | 3.812 | 3.608 | 3.944 | 3.978 | 4.057 | 1.645 | 1.724 | 2.051 |
| Total | 19.831 | 19.760 | 19.625 | 19.755 | 19.748 | 19.826 | 19.779 | 19.853 | 19.866 | 19.794 |
| $X_{Fe}$ | 0.603 | 0.592 | 0.544 | 0.577 | 0.550 | 0.539 | 0.531 | 0.808 | 0.791 | 0.754 |

Table 3 Rim compositions of chloritoid in lateritic metapelites.

| Subzone | Upper paragonite | | Lower andalusite | | | | |
|---|---|---|---|---|---|---|---|
| Sample | 509-04 | Karo-08 | 1118-24 | 1118-25 | Shi-11b | 509-06 | 509-07 |
| Assemblage | L2 | L2 | L3 | L4 | L4 | L4 | L5 |
| $SiO_2$ | 24.43 | 25.25 | 24.46 | 24.20 | 24.19 | 24.75 | 24.09 |
| $Al_2O_3$ | 40.29 | 41.02 | 40.82 | 40.17 | 40.85 | 41.09 | 40.93 |
| FeO | 25.50 | 25.05 | 26.26 | 26.91 | 25.84 | 24.71 | 28.11 |
| MgO | 1.86 | 1.87 | 1.45 | 1.15 | 1.51 | 2.22 | 0.84 |
| MnO | 0.50 | 0.39 | 0.18 | 0.21 | 0.10 | 0.10 | 0.28 |
| Total | 92.57 | 83.58 | 93.17 | 92.64 | 92.49 | 92.87 | 94.25 |
| Numbers of cations on the basis of 6 oxygens | | | | | | | |
| Si | 1.014 | 1.030 | 1.010 | 1.010 | 1.004 | 1.016 | 0.993 |
| Al | 1.970 | 1.972 | 1.986 | 1.975 | 1.999 | 1.988 | 1.989 |
| Fe | 0.885 | 0.855 | 0.906 | 0.939 | 0.897 | 0.848 | 0.969 |
| Mn | 0.017 | 0.013 | 0.006 | 0.007 | 0.004 | 0.003 | 0.010 |
| Mg | 0.115 | 0.114 | 0.089 | 0.072 | 0.093 | 0.136 | 0.052 |
| Total | 4.001 | 3.984 | 3.997 | 4.003 | 3.997 | 3.991 | 4.012 |
| $X_{Fe}$ | 0.870 | 0.883 | 0.910 | 0.929 | 0.906 | 0.862 | 0.949 |

*al.*, 1977), is introduced in the cordierite structure by a substitution silimar to edenite substitution in amphiboles (□ Si⇄NaAl).

IR spectra of three cordierites from the upper andalusite subzone indicate the presence of water molecule. The water contents in these cordierites are estimated by measuring refractive indices (Lepezin *et al.*, 1976) (Fig. 5). Cordierite in one sample was further examined by DTA. The estimated water contents are 0.5-2wt%, corresponding to about 0.2-0.8 molecule per formula unit.

### 4.4 Garnet

Garnet is Fe-rich with almandine content more than 83mol% (Table 5). Grossular content is low (2-4mol%) and is almost constant within a grain. The Mn, Mg and Fe contents vary systematically in garnet grains. The spes sartine component decreases very slightly from core to rim. Fe also decreases slightly from core to rim. Conversely, Mg increases very slightly from core to rim. Fe is locally enriched at resorbed edges of garnet in contact with decussate aggregate of biotite.

### 4.5 Biotite

Biotite (Table 6) is relatively high in Al content and low in Ti content as compared to those in some medium- and low-pressure metapelites (Guidotti, 1984; Guidotti *et al.*, 1988). The total numbers of octahedral cations are significantly smaller than the ideal number (6, at O = 22) in biotite coexisting with muscovite. This suggests an extensive muscovite solid solution in biotite. Biotite in the lateritic metapelite is exceedingly Fe-rich; the most ferruginous one has $X_{Fe}$ as high as 0.83.

Table 4 Microprobe analyses of cordierite.

| | Upper andalusite subzone | | | | | | Lower sillimanite subzone | | | Upper sillimanite subzone | | | |
|---|---|---|---|---|---|---|---|---|---|---|---|---|---|
| Sample | 906-37 | Ft-3 | 616-01 | Ft-7 | Wak-19c | 616-04 | Wak-135 | Kom-355 | 616-11 | Ak-12c | Ak-12b | Ft-19 | Ak-15 |
| Assemblage | A4 | A4 | A4 | A4 | A5 | A5 | A6 | A6 | A6 | A6 | A7 | A7 | A7' |
| $SiO_2$ | 47.55 | 48.16 | 48.07 | 48.01 | 47.83 | 47.92 | 47.90 | 47.51 | 47.86 | 47.20 | 47.78 | 48.01 | 47.57 |
| $Al_2O_3$ | 32.92 | 33.66 | 32.24 | 32.95 | 32.32 | 32.57 | 32.33 | 32.77 | 32.28 | 31.94 | 32.74 | 32.97 | 31.94 |
| FeO | 10.53 | 10.45 | 10.27 | 10.13 | 11.57 | 11.37 | 11.26 | 12.16 | 12.68 | 14.98 | 11.71 | 10.00 | 13.61 |
| MnO | 0.30 | 0.21 | 0.34 | 0.22 | 0.18 | 0.13 | 0.33 | 0.32 | 0.14 | 0.27 | 0.14 | 0.16 | 0.22 |
| MgO | 7.01 | 7.25 | 7.28 | 7.51 | 7.09 | 6.72 | 6.27 | 6.30 | 5.81 | 4.52 | 6.52 | 7.35 | 5.24 |
| CaO | tr | 0.10 | 0.09 | 0.08 | tr | tr | tr | tr | 0.02 | 0.08 | 0.12 | 0.12 | 0.14 |
| $Na_2O$ | 0.37 | 0.26 | 0.35 | 0.28 | 0.15 | 0.35 | 0.26 | 0.25 | 0.32 | 0.12 | 0.17 | 0.37 | 0.19 |
| Total | 98.68 | 99.09 | 98.64 | 99.18 | 99.14 | 99.06 | 98.35 | 99.31 | 99.11 | 99.11 | 99.18 | 98.98 | 98.91 |
| | Numbers of cations on the basis of 18 oxygens | | | | | | | | | | | | |
| Si | 4.942 | 4.978 | 4.993 | 4.953 | 4.967 | 4.974 | 5.005 | 4.942 | 4.994 | 4.981 | 4.961 | 4.959 | 4.998 |
| $^{IV}Al$ | 1.058 | 1.022 | 1.007 | 1.047 | 1.033 | 1.026 | 0.995 | 1.058 | 1.006 | 1.019 | 1.039 | 1.041 | 1.002 |
| $^{VI}Al$ | 2.976 | 2.957 | 2.940 | 2.959 | 2.922 | 2.959 | 2.987 | 2.960 | 2.961 | 2.954 | 2.967 | 2.974 | 2.953 |
| Fe | 0.915 | 0.903 | 0.892 | 0.874 | 1.005 | 0.987 | 0.984 | 1.058 | 1.107 | 1.322 | 1.017 | 0.864 | 1.196 |
| Mn | 0.026 | 0.018 | 0.030 | 0.019 | 0.016 | 0.011 | 0.029 | 0.028 | 0.012 | 0.024 | 0.012 | 0.014 | 0.020 |
| Mg | 1.086 | 1.117 | 1.127 | 1.155 | 1.097 | 1.040 | 0.977 | 0.977 | 0.904 | 0.711 | 1.009 | 0.132 | 0.821 |
| Ca | — | 0.011 | 0.010 | 0.009 | — | — | — | — | 0.002 | 0.009 | 0.013 | 0.013 | 0.016 |
| Na | 0.075 | 0.052 | 0.070 | 0.056 | 0.030 | 0.070 | 0.053 | 0.050 | 0.065 | 0.025 | 0.034 | 0.074 | 0.039 |
| Total | 11.078 | 11.059 | 11.069 | 11.072 | 11.071 | 11.068 | 11.030 | 11.074 | 11.053 | 11.045 | 11.053 | 11.071 | 11.044 |
| $X_{Fe}$ | 0.457 | 0.447 | 0.442 | 0.431 | 0.478 | 0.487 | 0.502 | 0.520 | 0.550 | 0.650 | 0.502 | 0.433 | 0.593 |

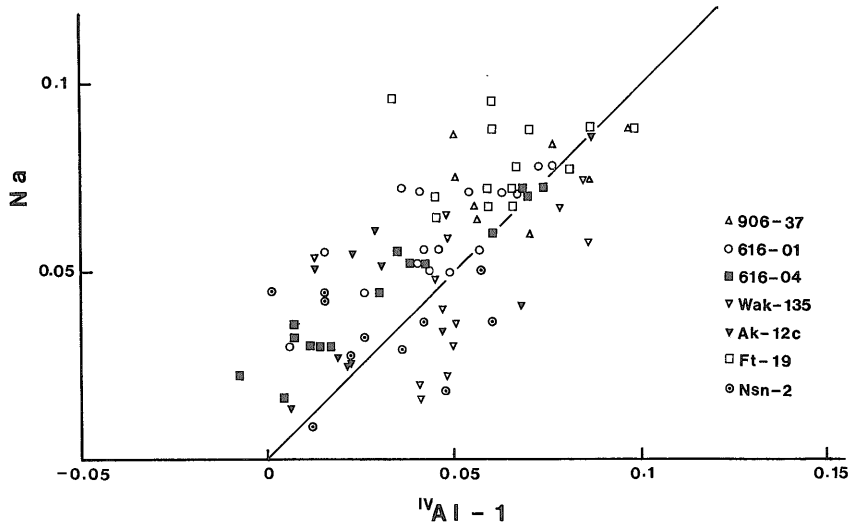


Fig. 4 Positive correlation between Na content and excess tetrahedral Al ($^{IV}$Al-1) in cordierite. The 1:1 line in the figure indicates compositional control by edenite-type substitution, □ Si⇄NaAl.

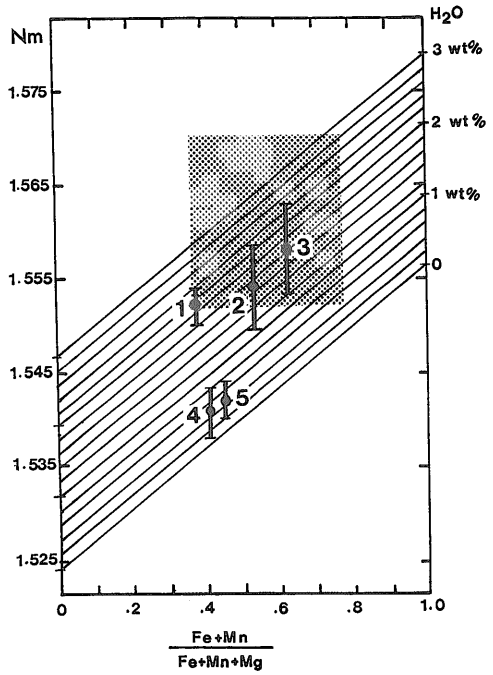


Fig. 5 Water contents in cordierite estimated from the (Fe + Mn)/(Fe + Mg + Mn) ratios and mean refractive indices, $N_m = (n_\alpha + n_\gamma)/2$ (a method of Lepetzin *et al.*, 1976). Samples: 1; Sum610-12b, 2;Mt-3, 3;Nkg-8a, 4;Wak-100, 5;Kom-355. The stippled area represents ranges in compositions and refractive indices of cordierite by Seki (1957).

Table 5 Rim compositions of garnet in high-grade hornfels of the Tono aureole.

| Subzone | Upper andalusite | Upper sillimanite | | |
|---|---|---|---|---|
| Sample | Shr-64 | Ak-12b | Ft-19 | Ak-15 |
| Assemblage | L7 | A7 | A7 | A7' |
| $SiO_2$ | 36.39 | 36.51 | 36.62 | 36.90 |
| $TiO_2$ | 0.02 | 0.05 | 0.02 | 0.07 |
| $Al_2O_3$ | 21.22 | 21.11 | 21.37 | 20.93 |
| FeO | 35.12 | 37.54 | 36.68 | 37.33 |
| MnO | 3.45 | 0.97 | 1.59 | 1.63 |
| MgO | 2.49 | 2.92 | 2.70 | 2.10 |
| CaO | 1.60 | 0.57 | 1.50 | 1.33 |
| Total | 100.28 | 99.97 | 100.48 | 100.29 |
| Atomic proportions on the basis of 8 cations | | | | |
| Si | 2.937 | 2.962 | 2.944 | 3.988 |
| Al | 2.019 | 2.018 | 2.025 | 1.998 |
| Ti | 0.001 | 0.003 | 0.001 | 0.004 |
| $Fe^{3+}$ | 0.097 | 0.043 | 0.075 | 0.008 |
| $Fe^{2+}$ | 2.273 | 2.504 | 2.389 | 2.521 |
| Mn | 0.236 | 0.067 | 0.108 | 0.112 |
| Mg | 0.299 | 0.353 | 0.324 | 0.254 |
| Ca | 0.138 | 0.050 | 0.129 | 0.115 |
| $X_{Fe}$ | 0.884 | 0.905 | 0.908 | 0.861 |

### 4.6 Muscovite

Muscovite in the study area is relatively high in Al content (Table 7). The excess Si (Si -6, at O = 22) changes concordantly with Fe + Mg in the octahedral site in muscovite of the Pg + Chl, Prl + Pg + Chl and And + Chl assemblages (Fig. 6). This indicates that Fe and Mg are introduced mainly by the celadonite solid solution. Judged from Si contents, the extent of celadonite solid solution in muscovite of the study area is relatively small as compared to that in the chlorite + muscovite assemblage from Ryoke and Sanbagawa metamorphic rocks (Wang *et al.*, 1986; Wang and Banno, 1988).

The amount of celadonite component increases with decreasing $X_{Fe}$ of coexisting chlorite in the biotite-free assemblages noted above (Fig. 6). This is consistent with chlorite composition that becomes slightly silicic with decreasing $X_{Fe}$ (Table 2). The amount of excess Si decreases distinctly with the formation of biotite, suggesting consumption of celadonite component. The Fe + Mg in the octahedral site, however, do not decrease but increase in muscovite coexisting with biotite. The amount of excess cations in the octahedral site (ideal number = 4, at O = 22) also increases with the sum of Fe and Mg. Note that the degree of octahedral deficiency of coexisting biotite is in a concordant relation

Table 6 Microprobe analyses of biotite.

| | Lower andalusite subzone | | | | | | | | | Upper andalusite subzone | | | |
|---|---|---|---|---|---|---|---|---|---|---|---|---|---|
| Sample | Man-39 | Man-40a | 906-39 | 611-06 | 906-38 | 1118-25 | Shi-11b | 509-06 | 509-07 | 906-37 | Ft-3 | 616-01 | Ft-7 |
| Assemblage | A3 | A3 | A3 | A3 | A3 | L4 | L4 | L4 | L5 | A4 | A4 | A4 | A4 |
| $SiO_2$ | 34.67 | 35.02 | 35.03 | 34.56 | 34.46 | 34.34 | 34.82 | 34.58 | 35.03 | 35.23 | 35.31 | 34.80 | 36.17 |
| $TiO_2$ | 1.15 | 1.18 | 1.22 | 1.42 | 1.33 | 1.28 | 1.11 | 1.76 | 1.58 | 1.85 | 2.46 | 1.97 | 1.86 |
| $Al_2O_3$ | 19.80 | 20.10 | 20.16 | 21.08 | 21.27 | 20.00 | 20.68 | 21.40 | 22.21 | 20.98 | 18.85 | 21.08 | 18.99 |
| FeO | 24.29 | 24.15 | 24.00 | 21.45 | 21.11 | 28.43 | 27.50 | 25.19 | 24.69 | 20.35 | 20.56 | 19.67 | 19.65 |
| MnO | 0.07 | 0.05 | tr | 0.11 | 0.05 | tr | tr | tr | tr | 0.12 | 0.20 | 0.03 | tr |
| MgO | 6.28 | 6.73 | 7.07 | 7.91 | 7.88 | 3.16 | 3.39 | 3.97 | 3.67 | 7.96 | 8.59 | 8.25 | 9.31 |
| CaO | 0.15 | 0.11 | 0.17 | 0.17 | 0.32 | 0.11 | 0.05 | 0.14 | 0.08 | 0.08 | 0.06 | 0.20 | 0.16 |
| $Na_2O$ | 0.24 | 0.29 | 0.35 | 0.22 | 0.46 | 0.31 | 0.22 | 0.57 | 0.22 | 0.29 | 0.25 | 0.20 | 0.25 |
| $K_2O$ | 8.77 | 8.72 | 8.62 | 8.98 | 8.72 | 8.45 | 8.71 | 8.91 | 8.60 | 8.85 | 9.03 | 9.15 | 9.20 |
| Total | 96.42 | 96.35 | 96.62 | 95.90 | 95.90 | 96.08 | 96.48 | 96.52 | 96.08 | 95.71 | 95.31 | 95.35 | 95.50 |
| | Numbers of cations on the basis of 22 oxygens | | | | | | | | | | | | |
| Si | 5.379 | 5.366 | 5.345 | 5.263 | 5.253 | 5.386 | 5.404 | 5.319 | 5.366 | 5.333 | 5.399 | 5.285 | 5.476 |
| $^{IV}Al$ | 2.621 | 2.634 | 2.655 | 2.737 | 2.747 | 2.614 | 2.596 | 2.681 | 2.634 | 2.667 | 2.601 | 2.715 | 2.524 |
| $^{VI}Al$ | 1.000 | 0.996 | 0.972 | 1.046 | 1.075 | 1.084 | 1.187 | 1.200 | 1.377 | 1.076 | 0.796 | 1.059 | 0.865 |
| Ti | 0.134 | 0.136 | 0.140 | 0.163 | 0.152 | 0.151 | 0.130 | 0.204 | 0.182 | 0.211 | 0.283 | 0.225 | 0.212 |
| Fe | 3.152 | 3.095 | 3.063 | 2.732 | 2.691 | 3.729 | 3.570 | 3.241 | 3.163 | 2.576 | 2.629 | 2.498 | 2.488 |
| Mn | 0.009 | 0.006 | — | 0.014 | 0.006 | — | — | — | — | 0.015 | 0.026 | 0.004 | — |
| Mg | 1.452 | 1.537 | 1.608 | 1.796 | 1.791 | 0.739 | 0.748 | 0.910 | 0.838 | 1.796 | 1.985 | 1.868 | 2.101 |
| Σ(VI) | 5.747 | 5.770 | 5.783 | 5.750 | 5.716 | 5.703 | 5.671 | 5.554 | 5.560 | 5.675 | 5.692 | 5.654 | 5.666 |
| Ca | 0.025 | 0.018 | 0.028 | 0.028 | 0.052 | 0.018 | 0.008 | 0.023 | 0.013 | 0.013 | 0.010 | 0.033 | 0.026 |
| Na | 0.072 | 0.086 | 0.104 | 0.065 | 0.136 | 0.094 | 0.066 | 0.170 | 0.065 | 0.085 | 0.074 | 0.059 | 0.073 |
| K | 1.736 | 1.705 | 1.678 | 1.745 | 1.696 | 1.691 | 1.725 | 1.794 | 1.681 | 1.709 | 1.761 | 1.773 | 1.777 |
| Σ(XII) | 1.833 | 1.809 | 1.810 | 1.837 | 1.884 | 1.803 | 1.799 | 1.942 | 1.759 | 1.807 | 1.845 | 1.864 | 1.876 |
| $X_{Fe}$ | 0.685 | 0.668 | 0.656 | 0.603 | 0.600 | 0.835 | 0.820 | 0.781 | 0.791 | 0.589 | 0.573 | 0.572 | 0.542 |

Table 6 (Continued)

| | Upper andalusite subzone | | | | Lower sillimanite subzone | | | Upper sillimanite subzone | | |
|---|---|---|---|---|---|---|---|---|---|---|
| Sample | Yks-7 | Wak-19c | 616-04 | Shr-64 | Wak-135 | Kom-355 | 616-11 | Ak-12c | Ak12b | Ft-19 |
| Assemblage | L6 | A5 | A5 | L7 | A6 | A6 | A6 | A7 | A7 | A7 |
| $SiO_2$ | 33.06 | 35.47 | 34.94 | 33.91 | 34.69 | 34.75 | 33.39 | 32.73 | 34.06 | 33.98 |
| $TiO_2$ | 2.51 | 1.88 | 2.11 | 2.02 | 2.77 | 3.04 | 3.01 | 3.00 | 3.07 | 2.82 |
| $Al_2O_3$ | 20.25 | 20.52 | 19.62 | 19.96 | 19.40 | 19.46 | 19.96 | 20.13 | 20.53 | 20.16 |
| FeO | 28.53 | 20.89 | 21.62 | 26.83 | 21.97 | 22.53 | 22.27 | 26.42 | 22.26 | 22.42 |
| MnO | 0.18 | 0.17 | tr | tr | 0.08 | 0.11 | 0.16 | 0.12 | tr | tr |
| MgO | 3.35 | 7.03 | 8.10 | 4.62 | 7.27 | 6.30 | 6.92 | 4.60 | 6.81 | 7.13 |
| CaO | 0.21 | 0.16 | 0.25 | 0.08 | 0.12 | 0.17 | 0.23 | 0.23 | 0.08 | 0.05 |
| $Na_2O$ | 0.21 | tr | 0.25 | 0.21 | 0.09 | 0.16 | 0.14 | 0.15 | 0.08 | 0.13 |
| $K_2O$ | 8.62 | 9.29 | 8.91 | 8.65 | 9.16 | 9.31 | 8.99 | 8.75 | 8.97 | 9.02 |
| Total | 96.92 | 95.69 | 95.81 | 96.28 | 95.55 | 95.83 | 96.07 | 96.13 | 95.87 | 95.71 |
| | Numbers of cations on the basis of 22 oxygens | | | | | | | | | |
| Si | 5.172 | 5.394 | 5.335 | 5.280 | 5.330 | 5.343 | 5.262 | 5.122 | 5.215 | 5.222 |
| $^{IU}Al$ | 2.828 | 2.606 | 2.665 | 2.720 | 2.670 | 2.657 | 2.738 | 2.878 | 2.785 | 2.778 |
| $^{UI}Al$ | 0.906 | 1.074 | 0.866 | 0.944 | 0.843 | 0.870 | 0.861 | 0.835 | 0.920 | 0.874 |
| Ti | 0.295 | 0.215 | 0.242 | 0.237 | 0.320 | 0.352 | 0.346 | 0.353 | 0.354 | 0.326 |
| Fe | 3.733 | 2.657 | 2.760 | 3.494 | 2.823 | 2.897 | 2.850 | 3.458 | 2.850 | 2.881 |
| Mn | 0.024 | 0.022 | — | — | 0.010 | 0.014 | 0.021 | 0.016 | — | — |
| Mg | 0.781 | 1.655 | 1.843 | 1.072 | 1.665 | 1.444 | 1.578 | 1.072 | 1.554 | 1.633 |
| Σ(VI) | 5.739 | 5.623 | 5.712 | 5.747 | 5.662 | 5.577 | 5.656 | 5.737 | 5.678 | 5.714 |
| Ca | 0.035 | 0.026 | 0.041 | 0.013 | 0.020 | 0.028 | 0.039 | 0.039 | 0.013 | 0.008 |
| Na | 0.064 | | 0.074 | 0.063 | 0.027 | 0.048 | 0.042 | 0.046 | 0.024 | 0.039 |
| K | 1.720 | 1.802 | 1.735 | 1.718 | 1.796 | 1.826 | 1.755 | 1.747 | 1.752 | 1.768 |
| Σ(XII) | 1.819 | 1.829 | 1.850 | 1.795 | 1.842 | 1.902 | 1.834 | 1.831 | 1.789 | 1.815 |
| $X_{Fe}$ | 0.827 | 0.616 | 0.600 | 0.765 | 0.629 | 0.667 | 0.644 | 0.763 | 0.647 | 0.638 |

Table 7 Microprobe analyses of muscovite.

| | Lower paragonite subzone | | | | Upper paragonite subzone | | | | | | Lower andalusite subzone | | | |
|---|---|---|---|---|---|---|---|---|---|---|---|---|---|---|
| Sample | 906-01 | 513-10 | 513-02 | Yag-282 | Karo-26 | 906-21 | Nak-154 | 509-04 | 514-01 | 509-05 | 611-03 | 1118-03 | 1118-24 | Man-39 |
| Assemblage | A1 | A1 | A1 | L1 | A1 | A1 | A1 | L2 | C | C | A2 | A2 | L3 | A3 |
| $SiO_2$ | 45.69 | 45.76 | 47.16 | 45.29 | 45.61 | 47.63 | 46.89 | 45.58 | 45.95 | 45.25 | 45.61 | 46.12 | 45.44 | 46.21 |
| $TiO_2$ | 0.17 | 0.22 | 0.22 | 0.17 | 0.18 | 0.23 | 0.27 | 0.13 | 0.15 | 0.09 | 0.18 | 0.20 | 0.20 | 0.11 |
| $Al_2O_3$ | 35.60 | 34.30 | 34.55 | 36.59 | 34.89 | 33.99 | 34.45 | 37.23 | 36.23 | 36.62 | 35.90 | 35.63 | 36.67 | 36.35 |
| FeO | 0.67 | 0.79 | 0.77 | 0.50 | 0.86 | 0.71 | 0.77 | 0.31 | 0.18 | 0.27 | 0.70 | 0.68 | 0.56 | 0.49 |
| MgO | 0.87 | 0.91 | 1.10 | 0.23 | 1.07 | 1.30 | 1.13 | 0.17 | 0.55 | 0.16 | 0.59 | 1.05 | 0.25 | 1.04 |
| CaO | 0.19 | 0.12 | 0.13 | 0.17 | 0.09 | 0.12 | 0.07 | 0.16 | 0.13 | 0.13 | 0.16 | 0.18 | 0.13 | 0.12 |
| $Na_2O$ | 0.82 | 0.91 | 0.87 | 0.89 | 1.26 | 0.92 | 0.99 | 1.25 | 1.14 | 1.31 | 1.67 | 1.09 | 1.01 | 1.19 |
| $K_2O$ | 9.92 | 9.69 | 9.88 | 10.01 | 9.34 | 10.03 | 9.96 | 9.45 | 9.48 | 9.42 | 8.85 | 9.61 | 9.92 | 9.47 |
| Total | 93.93 | 92.70 | 94.68 | 93.85 | 92.75 | 94.93 | 94.53 | 94.28 | 94.09 | 93.25 | 93.66 | 94.59 | 94.18 | 94.98 |
| Numbers of cations on the basis of 22 oxygens | | | | | | | | | | | | | | |
| Si | 6.138 | 6.226 | 6.276 | 6.086 | 6.165 | 6.326 | 6.259 | 6.074 | 6.112 | 6.042 | 6.129 | 6.147 | 6.084 | 6.119 |
| $^{IV}Al$ | 1.862 | 1.774 | 1.724 | 1.914 | 1.835 | 1.674 | 1.741 | 1.926 | 1.888 | 1.958 | 1.871 | 1.853 | 1.916 | 1.881 |
| $^{VI}Al$ | 3.775 | 3.726 | 3.696 | 3.881 | 3.703 | 3.646 | 3.679 | 3.921 | 3.790 | 3.805 | 3.814 | 3.744 | 3.872 | 3.793 |
| Ti | 0.017 | 0.023 | 0.022 | 0.017 | 0.018 | 0.023 | 0.027 | 0.013 | 0.015 | 0.009 | 0.018 | 0.020 | 0.020 | 0.011 |
| Fe | 0.075 | 0.090 | 0.086 | 0.056 | 0.097 | 0.079 | 0.086 | 0.035 | 0.020 | 0.030 | 0.079 | 0.076 | 0.063 | 0.054 |
| Mg | 0.174 | 0.185 | 0.218 | 0.046 | 0.216 | 0.257 | 0.225 | 0.034 | 0.109 | 0.032 | 0.118 | 0.209 | 0.050 | 0.205 |
| Σ(VI) | 4.042 | 4.024 | 4.022 | 4.001 | 4.034 | 4.006 | 4.017 | 4.002 | 3.934 | 3.878 | 4.029 | 4.048 | 4.005 | 4.063 |
| Ca | 0.027 | 0.009 | 0.019 | 0.024 | 0.013 | 0.017 | 0.010 | 0.023 | 0.019 | 0.019 | 0.016 | 0.026 | 0.019 | 0.017 |
| Na | 0.214 | 0.240 | 0.225 | 0.223 | 0.330 | 0.237 | 0.256 | 0.323 | 0.364 | 0.339 | 0.388 | 0.282 | 0.262 | 0.306 |
| K | 1.700 | 1.682 | 1.678 | 1.716 | 1.670 | 1.699 | 1.696 | 1.606 | 1.608 | 1.604 | 1.544 | 1.639 | 1.695 | 1.600 |
| Σ(XII) | 1.941 | 1.939 | 1.921 | 1.972 | 1.953 | 1.953 | 1.962 | 1.952 | 1.990 | 1.962 | 1.948 | 1.947 | 1.975 | 1.922 |
| $X_K$ | 0.876 | 0.867 | 0.873 | 0.870 | 0.824 | 0.870 | 0.864 | 0.823 | 0.808 | 0.818 | 0.767 | 0.842 | 0.858 | 0.832 |
| $X_{Na}$ | 0.110 | 0.124 | 0.117 | 0.118 | 0.169 | 0.121 | 0.131 | 0.165 | 0.183 | 0.173 | 0.221 | 0.145 | 0.133 | 0.159 |
| $X_{Ca}$ | 0.014 | 0.009 | 0.010 | 0.012 | 0.007 | 0.009 | 0.005 | 0.012 | 0.009 | 0.009 | 0.012 | 0.013 | 0.009 | 0.022 |

Table 7 (Continued)

| | Lower andalusite subzone (continued) | | | | | | | | | | Upper andalusite subzone | | | | |
|---|---|---|---|---|---|---|---|---|---|---|---|---|---|---|---|
| Sample | Man-40a | Man-40b | 906-39 | 611-04 | 611-06 | 906-38 | 1118-25 | Shi-11b | 509-06 | 509-07 | 906-37 | Ft-3 | 616-01 | Ft-7 | Yks-7 |
| Assemblage | A3 | A4 | A4 | A4 | A4 | A4 | L4 | L4 | L4 | L5 | A5 | A5 | A5 | A5 | L6 |
| $SiO_2$ | 46.04 | 45.91 | 45.81 | 45.21 | 45.49 | 45.12 | 45.01 | 44.61 | 44.27 | 44.19 | 45.10 | 45.02 | 44.72 | 44.57 | 44.13 |
| $TiO_2$ | 0.29 | 0.20 | 0.29 | 0.34 | 0.30 | 0.28 | 0.22 | 0.27 | 0.27 | 0.26 | 0.50 | 0.31 | 0.48 | 0.44 | 0.41 |
| $Al_2O_3$ | 35.95 | 35.94 | 35.93 | 35.38 | 35.40 | 35.48 | 35.99 | 35.25 | 35.26 | 35.17 | 36.41 | 36.09 | 35.83 | 37.05 | 35.79 |
| FeO | 0.48 | 0.40 | 0.58 | 0.58 | 0.57 | 0.58 | 1.49 | 2.15 | 2.60 | 2.91 | 0.66 | 0.89 | 0.79 | 0.66 | 2.69 |
| MgO | 1.11 | 0.61 | 1.49 | 1.61 | 1.47 | 1.91 | 0.62 | 1.04 | 1.24 | 1.30 | 1.18 | 1.65 | 1.70 | 0.48 | 1.15 |
| CaO | 0.17 | 0.14 | 0.28 | 0.11 | 0.21 | 0.43 | 0.10 | 0.12 | 0.11 | 0.26 | 0.12 | 0.23 | 0.15 | 0.15 | 0.20 |
| $Na_2O$ | 1.18 | 1.35 | 1.12 | 1.12 | 1.22 | 1.00 | 1.13 | 1.04 | 0.87 | 0.87 | 0.85 | 0.92 | 0.60 | 0.52 | 0.71 |
| $K_2O$ | 9.41 | 9.12 | 9.55 | 9.66 | 9.49 | 9.63 | 9.55 | 9.90 | 10.11 | 10.05 | 9.74 | 9.82 | 10.03 | 10.41 | 10.11 |
| Total | 94.63 | 93.67 | 95.05 | 94.01 | 94.12 | 94.43 | 94.11 | 94.40 | 94.73 | 95.01 | 94.56 | 94.90 | 94.30 | 94.28 | 95.19 |
| Numbers of cations on the basis of 22 oxgens | | | | | | | | | | | | | | | |
| Si | 6.122 | 6.152 | 6.080 | 6.075 | 6.095 | 6.042 | 6.058 | 6.030 | 5.985 | 5.970 | 6.021 | 6.006 | 6.005 | 5.983 | 5.939 |
| $^{IU}Al$ | 1.878 | 1.848 | 1.920 | 1.925 | 1.905 | 1.958 | 1.942 | 1.970 | 2.015 | 2.030 | 1.979 | 1.994 | 1.995 | 2.017 | 2.061 |
| $^{UI}Al$ | 3.756 | 3.828 | 3.700 | 3.678 | 3.689 | 3.642 | 3.768 | 3.645 | 3.604 | 3.570 | 3.750 | 3.682 | 3.675 | 3.846 | 3.616 |
| Ti | 0.029 | 0.020 | 0.029 | 0.034 | 0.030 | 0.028 | 0.022 | 0.027 | 0.027 | 0.026 | 0.050 | 0.031 | 0.048 | 0.044 | 0.041 |
| Fe | 0.053 | 0.045 | 0.064 | 0.065 | 0.064 | 0.065 | 0.168 | 0.245 | 0.294 | 0.329 | 0.074 | 0.096 | 0.089 | 0.074 | 0.303 |
| Mg | 0.218 | 0.122 | 0.295 | 0.322 | 0.294 | 0.381 | 0.124 | 0.210 | 0.250 | 0.262 | 0.235 | 0.328 | 0.340 | 0.096 | 0.231 |
| Σ(VI) | 4.058 | 4.015 | 4.089 | 4.099 | 4.077 | 4.116 | 4.083 | 4.128 | 4.176 | 4.186 | 4.108 | 4.137 | 4.153 | 4.060 | 4.191 |
| Ca | 0.024 | 0.020 | 0.040 | 0.016 | 0.030 | 0.062 | 0.014 | 0.017 | 0.016 | 0.038 | 0.017 | 0.033 | 0.022 | 0.022 | 0.029 |
| Na | 0.304 | 0.351 | 0.288 | 0.292 | 0.317 | 0.260 | 0.295 | 0.273 | 0.228 | 0.228 | 0.220 | 0.238 | 0.156 | 0.135 | 0.185 |
| K | 1.596 | 1.559 | 1.617 | 1.656 | 1.623 | 1.645 | 1.640 | 1.707 | 1.744 | 1.732 | 1.659 | 1.671 | 1.718 | 1.783 | 1.736 |
| Σ(XII) | 1.925 | 1.930 | 1.945 | 1.964 | 1.971 | 1.966 | 1.949 | 1.997 | 1.988 | 1.998 | 1.896 | 1.942 | 1.896 | 1.940 | 1.950 |
| $X_K$ | 0.829 | 0.808 | 0.831 | 0.843 | 0.824 | 0.837 | 0.841 | 0.855 | 0.877 | 0.867 | 0.875 | 0.861 | 0.906 | 0.919 | 0.890 |
| $X_{Na}$ | 0.158 | 0.182 | 0.148 | 0.149 | 0.161 | 0.132 | 0.151 | 0.136 | 0.115 | 0.114 | 0.112 | 0.123 | 0.082 | 0.070 | 0.095 |
| $X_{Ca}$ | 0.013 | 0.010 | 0.020 | 0.008 | 0.015 | 0.031 | 0.007 | 0.009 | 0.008 | 0.019 | 0.009 | 0.017 | 0.011 | 0.011 | 0.015 |

with the amount of excess octahedral cations in muscovite (Fig. 6). This suggests that the contents of Fe + Mg in muscovite is determined in the pseudobinary solid solution equilibria, with coexisting biotite. This solid solution is extensive in muscovite coexisting with Fe-rich biotite. Fig. 6 shows that Fe + Mg and octahedral excess in muscovite, and octahedral deficiency in biotite increase systematically with increasing $X_{Fe}$ of coexisting biotite (and chlorite).

Na content in muscovite of the paragonite zone is relatively high due to the solid solution with coexisting paragonite (Table 7). Na content increases toward high temperatures in the paragonite zone.

### 4.7 Paragonite and pyrophyllite

About 75% of metapelitic rocks of the paragonite zone contain paragonite so much as to be detected by X-ray diffraction. Paragonite contains very small amounts of Fe, Mg, Ca and Ti (Table 8). With increasing Na content in muscovite, K content in coexisting paragonite also increases concomitantly. Pyrophyllite is virtually pure hydrous aluminosilicate, with minor Fe as a detectable impurity.

### 4.8 Other phases

Metapelitic rocks treated here commonly contain $Al_2SiO_5$ polymorphs (andalusite or sillimanite), feldspars, Ti-phase, Fe sulfides and carbonaceous material (or graphite) together with Fe-Mg silicates and muscovite. Andalusite and sillimanite contain very limited amounts of Fe (less than 0.8wt% and 0.3wt%, respectively, in $Fe_2O_3$). Mn is below the detection limit in andalusite of this locality.

Plagioclase in aluminous metapelites of the paragonite zone is albite (An 0-3). In the

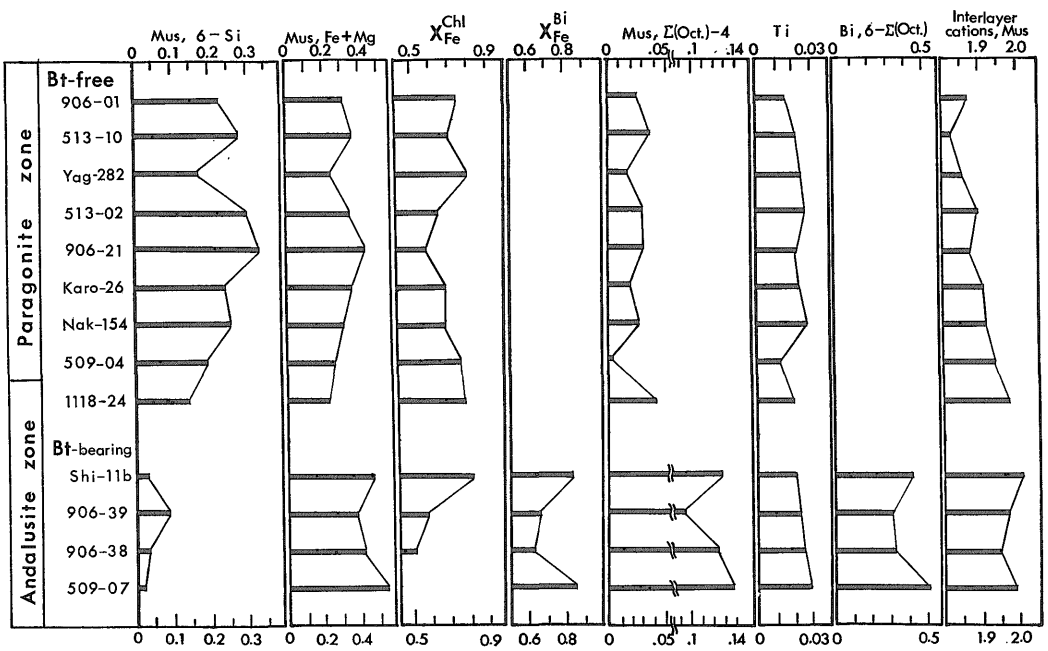


Fig. 6 Compositions of selected muscovites in the paragonite and andalusite zones. The absolute amounts of Fe and Mg in muscovite do not change significantly with the biotite formation. The amounts of excess Si and the excess cations in the octahedral site of muscovite, however, change distinctly with the biotite formation. All of these properties are in strong correlation with $X_{Fe}$ of coexisting chlorite and/or biotite.

Table 8 Microprobe analyses of paragonite and pyrophyllite.

| | Lower paragonite subzone | | | | | Upper paragonite subzone | | | |
|---|---|---|---|---|---|---|---|---|---|
| Sample | 906-01 | 513-10 | 513-02 | Yag-282 | | Karo-26 | 906-21 | Nak-154 | 509-04 |
| Assemblage | A1 | A1 | A1 | L1 | | A1 | A1 | A1 | L2 |
| Mineral | Pg | Pg | Pg | Pg | Prl | Pg | Pg | Pg | Pg |
| $SiO_2$ | 46.70 | 46.84 | 46.57 | 46.43 | 65.97 | 46.46 | 46.50 | 46.67 | 46.42 |
| $TiO_2$ | 0.11 | 0.15 | 0.11 | 0.08 | — | 0.10 | 0.11 | 0.19 | 0.15 |
| $Al_2O_3$ | 38.94 | 38.85 | 38.93 | 38.87 | 27.73 | 38.65 | 38.47 | 38.65 | 38.63 |
| FeO | 0.10 | 0.11 | 0.07 | 0.14 | 0.57 | 0.08 | 0.08 | 0.11 | 0.12 |
| MgO | 0.17 | 0.21 | 0.14 | 0.05 | — | 0.23 | 0.20 | 0.21 | 0.06 |
| CaO | 0.13 | 0.11 | 0.14 | 0.12 | — | 0.10 | 0.15 | 0.16 | 0.12 |
| $Na_2O$ | 7.39 | 7.35 | 7.19 | 7.54 | 0.08 | 7.01 | 7.04 | 7.25 | 7.16 |
| $K_2O$ | 0.51 | 0.61 | 0.76 | 0.60 | — | 0.77 | 0.84 | 0.92 | 0.94 |
| Total | 94.05 | 94.23 | 93.91 | 93.83 | 94.35 | 93.40 | 93.39 | 94.16 | 93.60 |
| | Numbers of cations on the basis of 22 oxygens | | | | | | | | |
| Si | 6.030 | 6.039 | 6.026 | 6.019 | 7.987 | 6.041 | 6.051 | 6.035 | 6.035 |
| $^{IU}Al$ | 1.970 | 1.961 | 1.974 | 1.981 | 0.017 | 1.959 | 1.949 | 1.965 | 1.965 |
| $^{UI}Al$ | 3.957 | 3.943 | 3.964 | 3.958 | 3.899 | 3.964 | 3.951 | 3.925 | 3.954 |
| Ti | 0.011 | 0.015 | 0.011 | 0.010 | — | 0.010 | 0.011 | 0.018 | 0.015 |
| Fe | 0.011 | 0.012 | 0.008 | 0.010 | 0.081 | 0.009 | 0.009 | 0.040 | 0.012 |
| Mg | 0.033 | 0.040 | 0.027 | 0.010 | — | 0.045 | 0.039 | 0.040 | 0.012 |
| Σ(VI) | 4.011 | 4.010 | 4.010 | 3.990 | 3.980 | 4.027 | 4.010 | 3.995 | 3.994 |
| Ca | 0.018 | 0.015 | 0.019 | 0.017 | — | 0.014 | 0.021 | 0.022 | 0.017 |
| Na | 1.850 | 1.838 | 1.804 | 1.895 | 0.006 | 1.767 | 1.776 | 1.818 | 1.805 |
| K | 0.084 | 0.100 | 0.125 | 0.099 | — | 0.128 | 0.139 | 0.151 | 0.156 |
| Σ(XII) | 1.952 | 1.953 | 1.949 | 2.011 | 0.006 | 1.909 | 1.936 | 1.991 | 1.977 |
| $X_K$ | 0.043 | 0.051 | 0.064 | 0.049 | — | 0.067 | 0.072 | 0.076 | 0.079 |
| $X_{Na}$ | 0.948 | 0.941 | 0.926 | 0.942 | — | 0.926 | 0.917 | 0.914 | 0.913 |
| $X_{Ca}$ | 0.009 | 0.008 | 0.010 | 0.008 | — | 0.007 | 0.011 | 0.011 | 0.008 |

lateritic metapelites, plagioclase (oligoclase) first appears in the uppermost of the upper paragonite subzone with the decomposition of paragonite. Plagioclase has compositions of An 17-29 in the andalusite zone and An 19-38 in the sillimanite zone. K-feldspar lacking exsolution texture has compositions of Or 85-89 in the upper andalusite subzone, Or 83-89 in the lower sillimanite subzone and Or 81-89 in the upper sillimanite subzone.

The Ti phase is sphene in the paragonite zone and ilmenite in the andalusite and sillimanite zones. Sphene contains less than 4 wt% $Al_2O_3$ and a minor amount of Fe. The presence of Al and the slight deficiency in total oxide suggest the presence of volatile component (cf. Franz and Spear, 1985). Ilmenite contains very small amounts of Mn, Mg and Al. Mag-netite and ilmenite coexist only in graphite-free, siliceous hornfels that are not discussed in this paper. The Fe sulfide phase is pyrite in the lower paragonite subzone and pyrrhotite

above the upper paragonite subzone. Carbonaceous material changes from coaly phytoclast to graphite through various types of transitional material (Okuyama-Kusunose and Itaya, 1987). Thus, in pelitic hornfels of the andalusite and sillimanite zones, coexisting ilmenite, pyrrhotite and gra-phite are the most common opaque assemblage.

## 5. Metamorphic reactions

The pelitic assemblages described above are treated in the model pelitic system $K_2O$-FeO-MgO-$Al_2O_3$-$SiO_2$-$H_2O$ (KFMASH). All the metapelites contain quartz and muscovite (or K-feldspar, above the decomposition of muscovite + quartz). The excess phases and components are pyrite and/or pyrrhotite for S, sphene or ilmenite for Ti, and carbonaceous material or graphite for C. Compositions of minerals used in balancing the reactions are idealized as shown in Table 9.

### 5.1 Reactions in aluminous metapelites

The changes in mineral assemblages in the aluminous metapelite described above are due to the systematic appearance and disappearance of minerals in the order of; And-in/Pg-out, Bt-in, Chl-out/Crd-in, Ms-out/Kfs-in, Sil-in and Alm-in. Mineral reactions responsible for these changes can be treated in the KFMASH model pelitic system and its subsystems. The exception is the formation of andalusite.

Andalusite appears with disappearance of paragonite. The mode of occurrence indicates a reaction relation;

$$Pg + 2Qtz = 2And + 2Ab + 2H_2O \quad (I).$$

The reaction is discontinuous in the system $Na_2O$-$Al_2O_3$-$SiO_2$-$H_2O$. The formation of andalusite from paragonite has a petrologic significance because paragonite is not considered as a source of $Al_2SiO_5$ polymorphs in common metapelitic rocks containing plagioclase.

The reactions for the Bt-in, Chl-out/Crd-in, Ms-out/Kfs-in, Sil-in and Alm-in are,

$$Chl + 2Ms = 2Bt + 5And + 3Qtz + 8H_2O \quad (a1)$$

$$2Chl + 2Ms + 9Qtz = 4Crd + And + 2Bt + 14H_2O \quad (III)$$

$$Ms + 2Qtz = 2And + 2Kfs + 2H_2O \quad (IV)$$

$$And = Sil \quad (V)$$

and

$$2Sil + Bt + 7Qtz = Alm + Crd + 2Kfs + 2H_2O \quad (VI),$$

respectively. Reactions labeled by Roman numbers are discontinuous and the others are continuous in the model pelitic system. In the observed assemblages, the univariant assemblages are very rare. Furthermore, most of the four-phase assemblages, such as the And + Bt + Crd + Chl and Alm + Bt + Crd + Sil assemblages, are containing secondary phases (chlorite or biotite) and are not considered true univariant assemblages.

Cordierite is formed by the reaction (III) which is a terminal equilibrium of chlorite. This is in contrast to most of the metapelites in the contact aureoles in which cordierite is produced by a continuous reaction between chlorite and muscovite (cf. the Ballachulish aureole, Pattison, 1989).

The characteristic assemblages in each subzone are constrained by continuous reactions in the model pelitic system. The example is the biotite-producing reaction (a1) and the assem blage (A3) in the lower andalusite subzone.

Table 9 Phase compositions used in balancing the equations.

| | | $Na_2O$ | $K_2O$ | $Al_2O_3$ | (Fe,Mg)O | $SiO_2$ | $H_2O$ |
|---|---|---|---|---|---|---|---|
| Chl | chlorite | 0 | 0 | 3 | 9 | 5 | 8 |
| Cld | chloritoid | 0 | 0 | 1 | 1 | 1 | 1 |
| Bt | biotite | 0 | 1 | 1.5 | 5.5 | 5.5 | 2 |
| Crd | cordierite | 0 | 0 | 2 | 2 | 5 | 0.5 |
| Alm | almandine | 0 | 0 | 1 | 3 | 3 | 0 |
| And | andalusite | 0 | 0 | 1 | 0 | 1 | 0 |
| Sil | sillimanite | 0 | 0 | 1 | 0 | 1 | 0 |
| Ms | musconvite | 0 | 1 | 3 | 0 | 6 | 2 |
| Pg | paragonite | 1 | 0 | 3 | 0 | 6 | 2 |
| Ab | albite | 0.5 | 0 | 0.5 | 0 | 3 | 0 |
| Kfs | K-feldspar | 0 | 0.5 | 0.5 | 0 | 3 | 0 |
| Qtz | quartz | 0 | 0 | 0 | 0 | 1 | 0 |

Figs. 7 to 9 are AFM diagrams projecting mineral compositions shown in the tables. Figs. 8 and 9 show that the three-phase fields And-Bt-Chl, And-Bt-Crd (+ Ms), and Alm-Bt-Crd gradually shift toward the Mg end in the AFM projection diagrams. This indicates that continuous reactions

$$Chl + 2Ms = 2Bt + 5And + 3Qtz + 8H_2O \quad (a1)$$

$$2Crd + 5Ms = 9And + 5Bt + 6Qtz + H_2O \quad (a2),$$

and

$$14Crd + 4Bt = 16Gt + 8Kfs + 12Qtz + 11H_2O \quad (a5)$$

begin from the Fe end and migrate to the Mg end, constraining the assemblages (A3), (A4) and (A7). Similarly, the shift in And/Sil-Bt-Crd (+ Kfs) fields in Figs. 8 and 9 also shows that the reactions,

$$16And/Sil + 4Bt + 42Qtz = 10Crd + 8Kfs + 3H_2O \quad (a3/a4)$$

constrain the compositional and modal changes of phases in the assemblages (A5) and (A6).

### 5.2 Mineral reactions in lateritic metapelites

Bulk compositions and the systematic change in mineral assemblages shown in the previous section indicate that the lateritic parageneses express the equilibria in Fe-rich portion of model pelitic system. In the stability field of muscovite + quartz, the mineral assemblages in the lateritic metapelite progressively change in the following order; (L1) Pg + Prl + Chl, (L2) Pg + Chl + Cld, (L3) Chl + Cld, (L4) Bt + Chl + Cld, (L5) And + Bt + Cld, and (L6) And + Bt. The changes of mineral assemblages can be described by reactions,

$$Chl + 3Prl = 9Cld + 20Qtz + 5H_2O \quad (b1)$$

$$Chl + 3Pg + 4Qtz = 9Cld + 6Pl + 5H_2O \quad (b2)$$

$$5Chl + 5Ms = 5Bt + 22Cld + 9Qtz + 21H_2O \quad (b3)$$

$$4Chl + 72Cld + 25Ms = 105And + 25Bt + Qtz + 102H_2O \quad (II)$$

and

$$5Cld + Ms + 6Qtz = 12And + Bt + 5H_2O \quad (b4),$$

that occur in this order. The field occurrence indicates that biotite is produced lower temperatures in the lateritic metapelite than in the aluminous metapelite. Biotite in the lateritic metapelite also appears in the lower andalusite subzone. The field relations indicate that the reactions (II), (a1) and (b3) must occur at slightly higher temperatures than reaction (I) producing andalusite. Moreover, the reaction (b3) occurs at lower temperatures than the reaction (a1) at the conditions of lower andalusite subzone of the Tono aureole.

Compositions of phases are also projected in

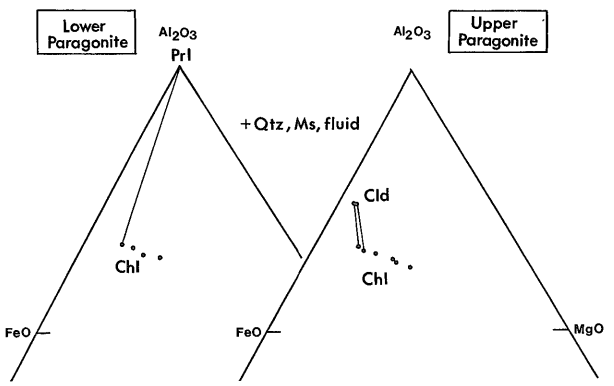


Fig. 7 AFM diagrams for mineral assemblages in metapelites of the paragonite zone. Metapelitic assemblages in the lower and upper subzones are shown by separate diagrams. In a strict sense, the assemblages are not fully treated in the KFMASH model pelitic system because of the overall presence of paragonite.

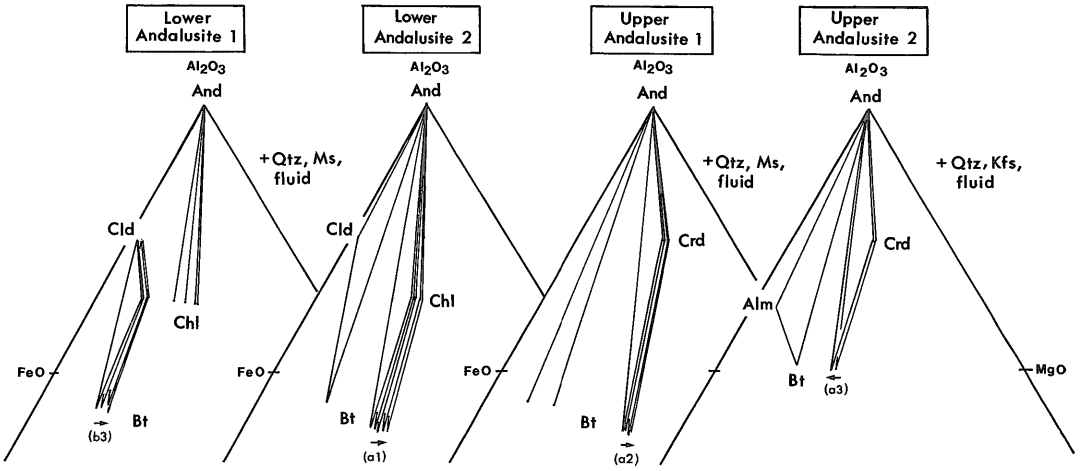


Fig. 8 AFM diagrams for mineral assemblages in metapelites of the andalusite zone. Metapelitic assemblages in the upper andalusite subzone are separately shown below and above the decomposition of muscovite + quartz which occurs in the uppermost of this subzone. Arrows in the figure indicate the direction of progressive shift of three-phase field for the assemblages (A3), (A4), (A5) and (L4) by the continuous reactions (a1), (a2), (a3) and (b4), respectively.

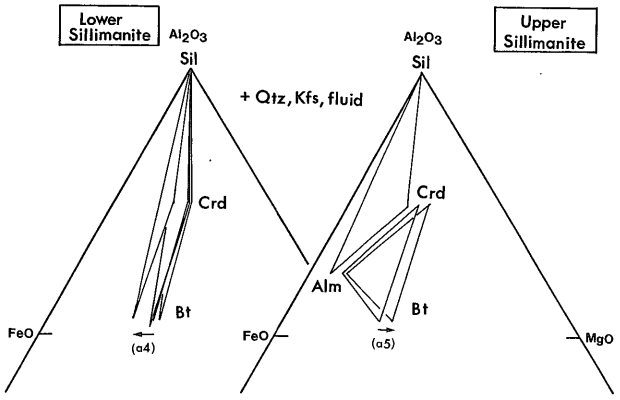


Fig. 9 AFM diagrams for mineral assemblages in metapelites of the sillimanite zone. Metapelitic assemblages in the lower and upper subzones are shown by separate diagrams. Arrows in the figure indicate the directions of progressive shift of three-phase field for the assemblages (A6) and (A7) by the continuous reactions (a4) and (a5), respectively.

a series of AFM diagrams (Figs. 7 to 9). Fig. 8 graphically shows that the chloritoid-bearing assemblages directly forms andalusite + biotite assemblage through the reaction (II). The operation of reaction (II) is a characteristic feature of typical low-pressure type metamorphism and will be discussed separately (Okuyama-Kusunose, in press.).

The $X_{Fe}$ of biotite in the And + Bt + Cld assemblage is always lower than $X_{Fe}$ of coexisting chloritoid. This indicates that the three-phase field constrained by the reaction (b4) migrates toward the Fe end of the AFM projection diagram. The reaction (b4) introduces

And + Bt two-phase assemblage in metapelitic system with slightly high Fe/(Fe + Mg) ratio. The reaction (a1) in the aluminous metapelite also produces the And + Bt assemblage. The And + Bt two-phase field extensively develops by the operation of these two reactions, separating chloritoid-bearing and chlorite-bearing three-phase fields for the lateritic and aluminous metapelites, respectively. The high-temperature limit of reaction (b4) is not confirmed by the field occurrence.

In the stability field of K-feldspar, phase relations in the lateritic metapelite is not well constrained due to the limited occurrence of this rock type. The occurrence of garnet-bearing assemblage (L7) indicate that a continuous reaction,

$$2And + 3Bt + 16Qtz = 5Alm + 6Kfs + 6H_2O \quad (b5)$$

took place in the Fe-rich pelitic rocks.

Although the relation among the reactions (b4), (b5), and the decomposition reaction of muscovite + quartz (IV) is not confirmed, these reactions impose a severe restriction on the occurrence of garnet-cordierite assemblage and staurolite in pelitic hornfels in the stability field of andalusite. Seki (1957) reported assemblages containing almandine garnet and cordierite in the upper andalusite subzone. However, this assemblage occurs only in the $K_2O$-poor, muscovite-absent hornfels (Okuyama-Kusunose, 1988). Uruno *et al.* (1986) reported that staurolite occurs in a garnet-cordierite hornfels of the Tono aureole. The second occurrence of staurolite in the Tono aureole is also from $K_2O$-poor metapelites (Okuyama-Kusunose *et al.*, 1991). The observed mineral assemblages in the Tono aureole indicate that the stable assemblage is the andalusite + Fe-rich biotite assemblage in Fe-rich metapelites of the low-pressure type metamorphism. The extensive stability of this assemblage, however, does not precludes staurolite in muscovite-bearing metapelites. The staurolite-bearing assemblage may be formed in bulk compositions with larger FeO/(FeO + MgO) ratio than the lateritic metape-lite (Table 1).

### 5.3 Schematic $T$-$X$ relations

The paragenetic changes in metapelites of the Tono contact metamorphic aureole are schematically shown in a series of AFM diagrams (Fig. 10). Based on the paragenetic changes, the shift of three-phase fields, and the observed order of reactions in progressive contact metamorphism, the reaction relations in the Tono aureole can be summarized in an isobaric $T$-$X_{Fe}$ diagram as shown in Fig. 11. The labeled reactions in Fig. 11 are those observed in the Tono aureole and is described in the previous section. The continuous reactions not labeled are,

$$Chl + Ms + Qtz = Bt + Crd + H_2O$$
$$Chl + Qtz = And + Crd + H_2O$$

and

$$Bt + Ms + Qtz = Crd + Kfs + H_2O.$$

The relative $T$-$X$ positions of these reactions to the reactions (a1), (a2), (III) and (IV) are studied by Labotka *et al.* (1981) and Pattison (1989), and are combined in Fig. 11. The paragenetic changes in the aluminous and lateritic metapelites of the study area are expressed in Fig. 11 along progressive paths in the intermediate to Fe-rich compositions.

## 6. Discussion

### 6.1 Importance of chloritoid and Fe-rich parageneses in low-pressure metamorphism

Pattison and Tracy (1991) proposed contact metamorphic facies series on the basis of metapelitic assemblages. They distinguished facies series characterized by the development of cordierite and andalusite (the facies series 1) and by a variety of assemblages of andalusite, sillimanite, cordierite and staurolite (the facies series 2). The facies series 1 is further subdivided into types 1a, 1b and 1c, by the absence, rare occurrence, and common occurrence, respectively, of sillimanite. Tono contact metamorphic aureole is classified into the type 1c aureole.

In the lateritic metapelite of the Tono aureole, chloritoid is an important rock forming mineral in a variety of assemblages with chlorite, andalusite and biotite. The andalu-

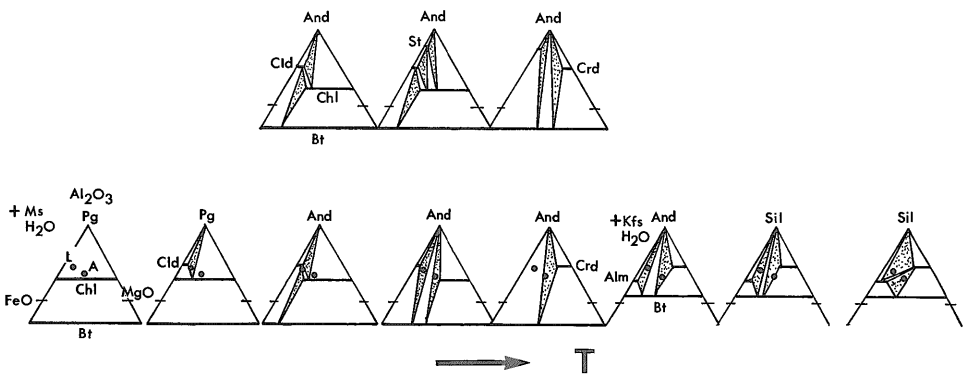


Fig. 10 Progressive changes of mineral assemblages in the Tono contact metamorphic aureole schematically shown in a series of AFM diagrams (the bottom array). The bulk compositions shown A and L indicate those of aluminous and lateritic metapelites. The AFM diagrams in the top array show the paragenetic changes of the low-pressure intermediate type (Miyashiro, 1961) compiled from the studies in the Panamint Mountains (Labotka, 1981) and the Bushveld aureole (Kaneko and Miyano, 1990).

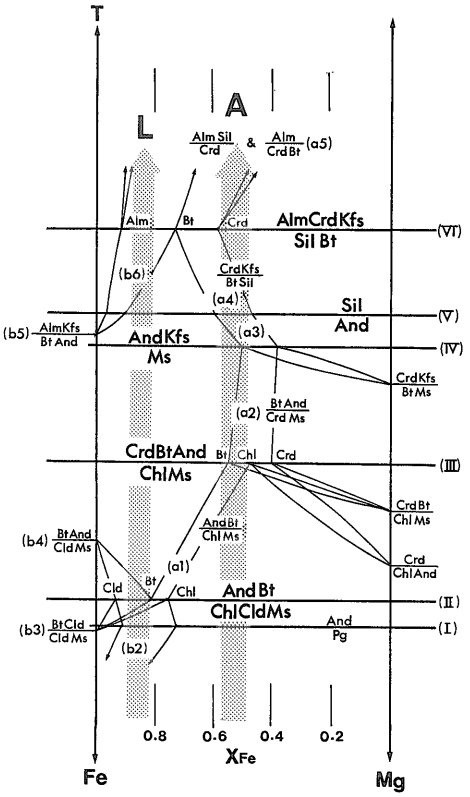


Fig. 11 Isobaric $T$-$X$ diagram for low-pressure type metapelites. The progressive path labeled A and L indicate those for the aluminous and lateritic metapelites of the Tono contact metamorphic aureole.

site + biotite assemblage is formed by the decomposition of chloritoid through andalusite + biotite + chloritoid assemblage. Besides the rather common occurrence of chloritoid, metapelites carrying staurolite and/or garnet do not occur in the stability of muscovite + quartz.

There are a few examples for chloritoid-bearing contact aureoles other than Tono aureole. These are the Santa Rosa aureole, Nevada (Compton, 1960), the Ardara aureole, northern Ireland (Pitcher and Berger, 1972), and the aureole around the Bushveld lopolith, South Africa (Kaneko and Miyano, 1990). These aureoles are the type 2 in the classification scheme of Pattison and Tracy (1991). Chloritoid also occurs in low- to middle-grade regional metapelites such as Stonehaven, Buchan Dalradian (Chinner, 1967), and Panamint Mountains, California (Labotka, 1981). Metamorphism in these localities is, however, low-pressure intermediate type (Miyashiro, 1961), and chloritoid eventually decomposes into andalusite + biotite + staurolite assemblage through chlorite + staurolite assemblage. Because of the discontinuous reaction (II), the chlorite + staurolite assemblage is never formed in the Tono aureole. The reaction (II) is also recognized in a contact metamorphic aureole in the Central Korea (Ahn and Na

kamura, 1990). The reaction (II) is probably a characteristic reaction only occurring in the typical low-pressure metamorphism.

### 6.2 Conditions of metamorphism in the Tono contact aureole

Tono contact metamorphic aureole is formed by the intrusion of Creataceous Tono granodiorite mass. The Cretaceous movement accompanied by the granitic intrusion (the Oshima orogenesis, by Kobayashi, 1941) largely determined the geologic structure presently exposed in the Kitakami Mountains. Tono mass as well as its contact aureole is partly disturbed by faulting in the later phase of this movement. However, there is no evidence of regional tilting in and after this movement. The study area comprises gently undulating hill with height of 300 to 700 m from the sea level. Thus, the contact metamorphism of the Tono aureole can be approximated to an isobaric process with negligible difference in pressures throughout the study area.

Metamorphism of pelitic rocks in the aureole is described by a combination of KFMASH reactions in a wide range of FeO/(FeO + MgO). An accumulation of thermodynamic data now enables calculation of a petrogenetic grid for metapelites. Calculated grids are recently proposed by Pattison (1989), Spear and Cheney (1989), Powell and Holland (1990), and Dymek and Sandiford (1992). All the calculated grids are, however, inconsistent to the observed phase relations in the Tono aureole, notably those involving chloritoid. The reasons for the failure of calculated grids probably lie in erroneous assumptions on the configuration of invariant points and in inaccuracy of thermodynamic parameters of Fe-Al silicates, such as chloritoid and staurolite (see discussion in Okuyama-Kusunose, in press.). Therefore, the estimation of metamorphic pressures and temperatures by using petrogenetic grid, an approach adopted by Pattison (1989), had to be abandoned in this study. The conditions of metamorphism in the Tono aureole are estimated through the dehydration equilibria of muscovite and paragonite and the andalusite-sillimanite transition combined with carbon isotopic geothermometer and garnet-bearing geothermobarometers.

#### 6.2.1 Carbon isotopic temperatures combined with andalusite-sillimanite transition and mica dehydrations

The andalusite-sillimanite transition occurred at higher temperatures than the reaction between muscovite and quartz. The progressive $P$-$T$ path of metamorphism, therefore, must pass below the intersection of muscovite + quartz dehydration curve and andalusite-sillimanite equilibrium. Furthermore, the metapelitic rocks of the Tono aureole underwent the paragonite + quartz dehydration reaction in the andalusite field. The isobaric intersection of progressive path with the paragonite + quartz equilibrium gives a temperature of beginning of the andalusite zone.

The dehydrations of muscovite and paragonite with quartz are fairly well constrained (Chatterjee, 1972; Chatterjee and Froese, 1975; Chatterjee and Flux, 1986). The position of the dehydration curves must be modified because metapelites studied here are all graphitic with dilution of hydrous metamorphic fluid by $CH_4$ and/or $CO_2$. The position of andalusite-sillimanite equilibrium is not precisely determined at present. The uncertainty for experimentally derived equilibrium curve is introduced mainly by the defects and minor element contents in two minerals (Kerrick, 1990). The geothermobarometric studies frequently provide consistent results with the $Al_2SiO_5$ equilibria by Holdaway (1971), and his andalusite-sillimanite curve is shown in the $P$-$T$ diagram of Fig. 12. Pattison (1989) argued, however, that the triple point by Holdaway (1971)'s equilibria is located in too much lower pressures. The empirical andalusite-sillimanite equilibrium proposed by him passes about 1 kbar higher pressures than that of Holdaway (1971), and is also presented in Fig. 12. Since petrologic grid by Pattison (1989) including his andalusite-sillimanite curve is internally consistent, it is presently assumed that the actual position of andalusite-sillimanite transition is between these two curves.

In the comparative study of metamorphic conditions with the Ryoke belt in the Chubu district, Central Japan, Morikiyo *et al.* (1989, 1992) measured carbon isotopic fractionation between graphite and calcite in the crystalline limestone of the Tono aureole. Crystalline limestone is abundant throughout the aureole, and the degree of $^{12}C/^{13}C$ fractionation ($\delta$ values) is determined at several locations where the key reactions are recognized. The $\delta$ values at the andalusite-sillimanite transition and the muscovite + quartz dehydration are 5.0 and 5.3, respectively (Morikiyo *et al.*, 1989). Based on these values of carbon isotopic fractionation, temperatures of 585°C, and 574°C, respectively, are calculated using carbon isotopic geothermometer calibrated by Morikiyo (1984). As muscovite + quartz dehydration occurs about 150-200 m low temperature side of And-Sil transition, the lateral thermal gradient in this part of the aureole is as high as 50-60°C/km.

The andalusite-sillimanite transition is univariant, and the pressure of phase transition can be fixed at a given temperature. The carbon isotopic temperature of andalusite-sillimanite transition (585°C) gives a pressure of about 2.3 kbar by the equilibrium curve of Holdaway (1971), and about 4.0 kbar by the equilibrium curve of Pattison (1989). Note that the dehydration of muscovite determined experimentally (Chatterjee and Flux, 1986) occurs at higher temperatures than the measured temperature by carbon isotopic thermometry (574°C), at pressures of 2.3 kbar and 4.0 kbar. This suggests that the activity of water ($a_{H_2O}$) in metamorphic fluid has been reduced significantly in graphitic metapelites treated here (see below).

The $\delta$ value at the paragonite + quartz dehydration is 13.0, and calculated temperature is 390°C. The temperature seems to be inconsistently low. Although carbonaceous material in crystalline limestone has completely graphitized (Morikiyo *et al.*, 1989), there is a possibility that the isotopic equilibrium has not been attained at temperatures below 500°C (Demeny and Kreulen, in press). The temperature at the paragonite + quartz dehydration does not, therefore, seem to be adequately estimated by the carbon isotopic thermometry. The andalusite isograd defined by the paragonite dehydration is located about 1.7-1.9 km away from the sillimanite isograd. Assuming a lateral thermal gradient of 50-60°C/km, the temperature at the andalusite isograd is about 90-100°C lower that the temperature at the sillimanite isograd. The temperature at the andalusite isograd is very roughly estimated to be around 490°C, on the basis of the temperature at the sillimanite isograd and the thermal gradient in the aureole.

### 6.2.2 Garnet-biotite and garnet-$Al_2SiO_5$-plagioclase-quartz geothermobarometry

The geothermobarometers involving garnet are applicable to metapelitic rocks of the upper andalusite and upper sillimanite subzones. The results are also shown in Fig. 12.

The temperatures are estimated by Hodges and Spear (1982)'s calibration of garnet-biotite geothermometer. The temperatures are about 670-720°C in the upper sillimanite subzone (Ak-12b and Ak-15) and about 600°C in the high-temperature part of the upper andalusite subzone (Shr-64). The estimated temperature for the upper andalusite subzone seems to be slightly high considering the measured temperature of andalusite-sillimanite transition. Because the estimated temperatures for the upper sillimanite subzone are rather consistent, this may imply that the And-Sil curve by Holdaway (1971) is placed in slightly lower pressures than its actual position. The garnet-biotite geothermometerby Indares and Martignole (1985) gives systematically lower temperatures than the estimations using the Hodges and Spear (1982)'s calibration. This may be due to low Ti contents of biotite in the study area as compared to the granulite facies rocks studies by Indares and Martignole (1985).

The pressures are also estimated by a garnet-$Al_2SiO_5$-plagioclase-quartz geobarometer applied for 2 samples. Calibration by Newton and Haselton (1981) is applied to the sillimanite-bearing Ak-15. Reymer *et al.*(1984) der-

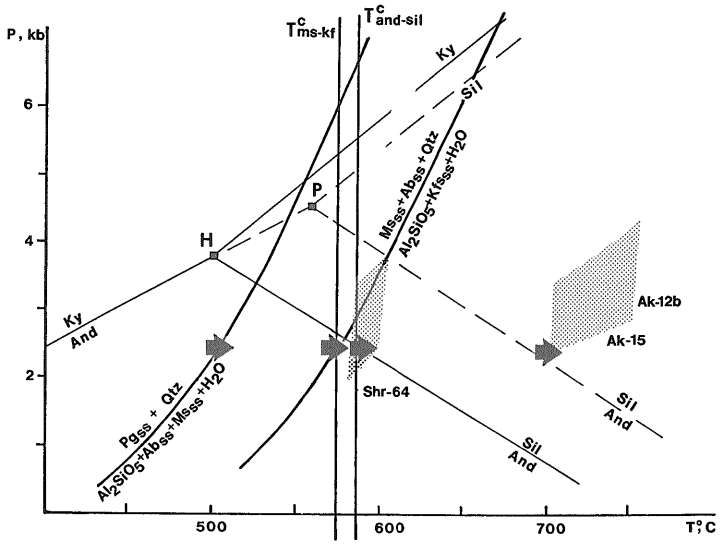


Fig. 12 Possible $P$-$T$ path of contact metamorphism in the Tono aureole (bold arrows). The conditions of metamorphism are estimated by the calcite-graphite carbon isotopic fractionation in limestone and the relation of muscovite + quartz dehydration and andalusite-sillimnaite transition. $T^c_{ms-kf}$ and $T^c_{and-sil}$ are the carbon isotopic temperatures at the muscovite + quartz dehydration and andalusite-sillimanite transition, respectively. The muscovite + quartz and paragonite + quartz dehydration curves are recalculated incorporating the effect of paragonite and muscovite solid solutions and the reduction of water activity in metamorphic fluid (Chatterjee and Flux, 1986). $Al_2SiO_5$ phase relations of Holdaway (1971) (H) and Pattison (1989) (P) are shown by solid and dashed lines, respectively. The dotted quadrilaterals show estimated range in pressures and temperatures by garnet-biotite geothermometer and garnet-$Al_2SiO_5$-plagioclase-quartz geobarometer. For the sample Shr-64 containing andalusite and biotite, the geobarometer and geothermometer can be applied all together. The results of geothermometry on the sample Ak-12b and of geobarometry on the sample Ak-15 are compiled for the conditions of upper sillimanite subzone. See text for the calibration used in the calculation.

ived a geobarometer for the andalusite-garnet plagioclase-quartz assemblage from the Newton and Haselton (1981)'s calibration and andalusite-sillimanite equilibrium by Holdaway (1971). This barometer is also applied to sample Shr-64 of the upper andalusite subzone. The estimated pressures range 2.1 to 3.5 kbar (Fig. 12). The results are broadly consistent with the two $Al_2SiO_5$ phase relations in that the estimated pressures are within the stability field of andalusite and sillimanite. The estimated pressures for Ak-15 combined with the garnet-biotite temperature of Ak-12b provides very limited room by the andalusite - sillimanite curve of by Pattison (1989).

### 6.2.3 Effect of reduced activity of $H_2O$ in fluid

The estimated temperature of the muscovite + quartz dehydration is exceedingly lower than the temperatures at 2.3 kbar on the experimentally determined equilibrium curves at $a_{H_2O}$ = 1.0 (Chatterjee and Froese, 1975; Chatterjee and Flux, 1986). The metapelites studied here all contain graphite (or carbonaceous matter, at low temperatures). This suggests that the temperatures of muscovite + quartz reaction is reduced due to an extensive dilution of metamorphic fluid by $CH_4$ and/or

$CO_2$.

The muscovite + quartz dehydration equilibrium of Chatterjee and Froese (1975) has been reexamined by Chatterjee and Flux (1986) based on the detailed study of muscovite-paragonite crystalline solution (Flux and Chatterjee, 1986). The carbon isotopic temperature is estimated to be 574°C at the muscovite + quartz dehydration. The muscovite + quartz dehydration equilibrium is studies using equation by Chatterjee and Flux (1986), and phase compositions in the samples Wak-19c (reactant assemblage) and Wak-135 (product assemblage). At a total pressure of 2.3 kbar estimated by Holdaway (1971)'s $Al_2SiO_5$ equilibria, the water activity of metamorphic fluid is calculated as low as $a_{H_2O} \simeq X_{H_2O} = 0.73$ at 574°C. At a total pressure of 3.9 kbar estimated by Pattison (1989)'s equilibria, the muscovite + quartz dehydration occurs at 574°C only with an extensively reduced water activity as low as $X_{H_2O} = 0.4$-0.5. Ohmoto and Kerrick (1977) and Ohmoto and Poulson (1989) studied fluid equilibria in the C-H-O-S system. The calculated fluid composition is around $X_{H_2O} = 0.7$-0.8 in a range in temperatures of 500-600°C and pressures of $P = 2$-4 kbar. The calculation is consistent to the estimated fluid composition based on the pressures by Holdaway (1971).

A quite similar result is also suggested for the paragonite + quartz dehydration. Based on Chatterjee and Flux (1986), the $X_{H_2O}$ in fluid in the paragonite + quartz reaction is estimated to be 0.78, a consistent value with the C-H-O-S fluid equilibria at 490°C and 2.3 kbar. The estimated fluid composition in the paragonite dehydration at conditions by Pattison (1989) (490°C, 4.0 kbar) is inconsistent to the calculated fluid equilibria in the C-H-O-S system. Moreover, there is a possibility that the $P$-$T$ conditions of paragonite dehydration estimated by Pattison (1989)'s equilibria fall in the stability field of kyanite in his $Al_2SiO_5$ equilibria. The discrepancy suggests that the pressures by Pattison (1989)'s And-Sil equilibrium is overestimated.

### 6.3 Importance of paragonite as a source of aluminosilicates

The widespread occurrence of andalusite is a characteristic feature of metapelites in the Tono contact metamorphic aureole. Pattison and Tracy (1991) classified the Tono aureole into the type 1c aureole based on the mode of occurrence of andalusite. The reaction producing andalusite in the model of Pattison and Tracy (1991) is similar to the reaction (a1) of this study.

Although the occurrence of andalusite apparently matches the model, the reaction truly responsible for the formation of andalusite in the Tono aureole is quite different to the idealized scheme by Pattison and Tracy (1991). Andalusite in the study area is formed by the reaction between paragonite and quartz as noted before. The reaction occurs in lower temperatures not only than the muscovite + quartz breakdown but also than the first appearance of biotite by reaction (a1). This may be a rare example that the breakdown of paragonite is confirmed in the stability field of andalusite.

The occurrence of paragonite in the low-grade zone of the Tono aureole is due to the aluminous bulk compositions of pelitic rocks (Okuyama, 1980; this study). Observed paragenetic relation indicates that the assemblage pyrophyllite + albite is not stable over paragonite in low-grade pelitic rocks. Although paragonite is relatively rare in low-pressure metapelites, the mode of occurrence in the Tono aureole suggests its importance as a source of aluminosilicates in the place of pyrophyllite.

## 7. Conclusions

(1) Pelitic metamorphic rocks in the contact aureole around the Cretaceous Tono granodiorite mass show systematic paragenetic changes with increasing temperatures. The aureole is divided into the paragonite, andalusite and sillimanite zones, on the basis of formation and phase transition of $Al_2SiO_5$ polymorphs. Each zone is further subdivided into upper and lower subzones by the formation of chloritoid, cordierite and almandine garnet.

(2) Most common type of pelitic rocks in the aureole (the aluminous metapelite) with bulk FeO/(FeO + MgO) ratio around 0.5-0.6 form typical low-pressure assemblages involving andalusite, sillimanite and cordierite. Metapelitic rocks with lateritic composition have bulk FeO/(FeO + MgO) as high as 0.86, and develop chloritoid-bearing assemblages.

(3) The reaction relations in the lateritic metapelite are characteristic that chloritoid directly decomposes into the andalusite + biotite in Fe-rich portion of the pelitic system. This relation is different from the reactions in the low-pressure intermediate type metamorphism in which chloritoid produces staurolite-bearing assemblages.

(4) Conditions of metamorphism are estimated by the carbon isotopic thermometry for limestones intercalating with metapelites, by the garnet-biotite geothermometer and garnet-$Al_2SiO_5$-plagioclase-quartz geobarometer, combined with $Al_2SiO_5$ equilibria. Metamorphism were conducted at an isobaric condition of 2.3 kbar. Temperatures were estimated to be lower than 490°C in the paragonite zone, 490°C to 600°C in the andalusite zone, 600°C to 670°C in the lower sillimanite subzone, and 670°C to 720°C in the upper sillimanite subzone. The fluid composition is estimated to be $X_{H_2O}$ = 0.7-0.8.

(5) The mode occurrence of paragonite suggests its importance as a source of aluminosilicates in metapelitic phase relations.

**Acknowledgements** : This paper is an outgrowth of my doctoral thesis submitted to Tohoku University. I would like to acknowledge gratefully Professor Kenichiro Aoki of Tohoku University and Professor Hitoshi Onuki of Hirosaki University for encouraging me to work in Sendai. Discussion with Dr. Toshiro Morikiyo of Shinshu University, and Dr. Yoshikuni Hiroi of Chiba University were very helpful. Dr. Michiaki Bunno of the Geological Museum, GSJ, kindly reviewed an earlier version of manuscript. The manuscript was further reviewed by Dr. T. Nakajima of the Geological Survey of Japan whose comments were grateful in improving the manuscript. The warm encouragement by Dr. Masaharu Kamitani and Dr. Yukio Sakamaki of the Geological Museum was greatly appreciated. Messers Shoji Abe, Yoshio Sato and I. Owada kindly supported me by preparing excellent thin sections.

## References

Ahn, K.S. and Nakamura, Y. (1990) The reaction chloritoid + chlorite + muscovite = biotite + andalusite + quartz + water in Fe-rich pelitic rocks. *Abstracts of 97 Annual Meeting (Toyama)*, Geological Society of Japan. p.478. (in Japanese)

Bluemel, P. and Schreyer, W. (1977) Phase relations in pelitic and psamitic gneisses of the sillimanite-potash feldspar and cordierite-potash feldspar zones in Moldanubicum of the LamBodenmais Area, Bavaria. *Jour. Petrol.*, vol. 18, p.431-459.

Chatterjee, N.D.(1972) The upper stability limit of the assem blage paragonite + quartz and its natural occurrences. *Contrib. Mineral. Petrol.*, vol.34, p. 288-303.

———— and Flux, S.(1986) Thermodynamic mixing properties of muscovite-paragonite crystalline solution at high temperatures and pressures, and their geologic applications. *Jour. Petrol.*, vol.27, p.677-693.

———— and Froese, E.(1975) A thermodynamic study of the pseudobinary join muscovite-paragonite in the system $KAlSi_3O_8$-$NaAlSi_3O_8$-$Al_2O_3$-$SiO_2$-$H_2O$. *Amer. Mineral.*, vol.60, p.985-993.

Chinner, G.A. (1967) Chloritoid, and the isochemical character of Barrow's zones. *Jour. Petrol.*, vol.8, p.268-282.

Compton, R.R. (1960) Contact metamorphism in Santa Rosa Range, Nevada. *Geol. Soc. Amer. Bull.*, vol.71, p.1383-1416.

Deer, W.A., Howie, R.A. and Zussman, J. (1982) Chloritoid. In *Rock forming minerals, 2nd ed.*, vol.1A; orthosili-

cates, p.867-912. Longmann, London.

Demeny, A. and Kreulen, R. (1991) Calcite-graphite isotopic exchange in Alpine Penninic rocks. (in press)

Dymoke, P. and Sandiford, M. (1992) Phase relationships in Buchan facies series pelitic assemblages: calculations with application to andalusite-staurolite parageneses in the Mount Lofty Ranges, South Australia. *Contrib. Mineral. Petrol.*, vol.110, p.121-132.

Ehiro, M. (1977) The Hizume-Kesennuma fault, with special reference to its character and significance on the geologic development. *Tohoku Univ. Inst. Geol. Paleont. Contrib.*, vol.77, p.1-37. (in Japanese with English abstract)

———— (1989) Mesozoic and Paleozoic Group. In Oide, K., Nakagawa, H. and Kanisawa, S. eds., *Tohoku District-Geology of Japan, 2*. p.7-73. (in Japanese)

Evans, N.H. and Speer, J.A. (1984) Low-pressure metamorphism and anatexis of Carolina Slate Belt phyllites in the contact aureole of the Lilesville Pluton, North Carolina, U.S.A. *Contrib. Mineral. Petrol.*, vol.87, p.297-309.

Flux, S. and Chatterjee, N.D. (1986) Experimental reversal of the Na-K exchange between muscovite-paragonite crystalline solution at 2 molal aqueous (Na,K)Cl fluid. *Jour. Petrol.*, vol.27, p.665-676.

Franz, G. and Spear, F.S. (1985) Aluminous titanite (sphene) from the eclogite zone, south-central Tauern Window, Austria. *Chem. Geol.*, vol. 50, p.33-46.

Fujimaki, H. and Aoki, K. (1980) Quantitative microanalyses of silicates, oxides and sulfides using an energy-dispersive type electron probe. *Sci. Rep. Tohoku Univ., Ser. III*, vol.14, p.261-268.

Gil Ibaruguchi, J.I. and Martinez, F.J. (1982) Petrology of garnet-cordierite-sillimanite gneisses from the El Tormes Thermal Dome, Iberian Hercynian Foldbelt (W. Spain). *Contrib. Mineral. Petrol.*, vol.80, p.14-24.

Goldman, D.S., Rossman, G.R. and Dollayse, W.A. (1977) Channel constituents in cordierite. *Amer. Mineral.*, vol. 62, p. 1144-1157.

Guidotti, C.V. (1984) Micas in metamorphic rocks. In Baily, S.W., ed., *Micas, Reviews in Mineralogy*, Vol. 13, p.357-467, Mineralogical Society of America, Washington DC.

————, Cheney, J.T. and Henry, D.J. (1988) Composi tional variation of biotite as a function of metamorphic reactions and mineral assemblage in the pelitic schists of Western Maine. *Amer. Jour. Sci.*, vol.288A, p.270-292.

Hodges, K.V. and Spear, F.S. (1982) Geothermometry, geobarometry and the $Al_2SiO_5$ triple point at Mt. Moosilauke, New Hampshire. *Amer. Mineral.*, vol. 67, p.1118-1134.

Holdaway, M.J. (1971) Stability of andalusite and the aluminum silicate phase diagram. *Amer. Jour. Sci.*, vol.271, p. 97-131.

Indares, A. and Martignole, J. (1985) Biotite-garnet geothermometry in the granulite facies: the influence of Ti and Al in biotite. *Amer. Mineral.*, vol. 70, p.272-287.

Kaneko, Y. and Miyano, T. (1990) Contact metamorphism by the Bushveld Complex in northern Transvaal, South Africa. *Jour. Mineral. Petrol. Econ. Geol.*, vol.85, p.66-81 (in Japanese with English abstract)

Kanisawa, S. and Ishikawa, K. (1987) Gabbroic rocks in the western margin of the Tono granitic mass, Kitakami Mountains. *Jour. Japan. Assoc. Mineral. Petrol. Econ. Geol.*, vol.82, p.162. (in Japanese)

———— and Katada, M. (1989) Characteristics of Early Creataceous igneous activity, Kitakami Mountains, Northeast Japan. *Earth Science (Chikyu Kagaku)*, vol.42, p.220-236.

————, Yoshida, T., Ishikawa, K. and Aoki, K. (1986) Geochemistry of the Tono

granitic mass, Kitakami Mountains. *Rept. Inst. Nuc. Sci., Tohoku Univ.*, vol.19, p.251-264. (in Japanese).

Katada, M. and Ono, C. (1968) Chemical compositions of pelitic rocks from the Paleozoic formations of the Kitakami Mountains, northeastern Japan. *Jour. Japan. Assoc. Mineral. Petrol. Econ. Geol.*, vol.60, p.75-91. (in Japanese)

Kawamura, M. (1985a) Lithostratigraphy of the Carboniferous Formations in the Setamai region, Southern Kitakami Mountains, Northeast Japan. (1) Shimoarisu district of the Setamai Subbelt. *Jour. Geol. Soc. Japan*, vol. 91, p.165-178. (in Japanese with English abstract)

———— (1985b) Lithostratigraphy of the Carboniferous Formations in the Setamai region, Southern Kitakami Mountains, Northeast Japan. (2) Karosawa and Oide district of the Omata Subbelt. *J. Geol. Soc. Japan*, vol. 91, p. 341-352. (in Japanese with English abstract)

Kawamura, T. and Kawamura, M. (1989) The Carboniferous System of the South Kitakami Terrane, northeast Japan. (II) Sedimentary and tectonic environment. *Earth Science (Chikyu Kagaku)*, vol.43, p.157-167. (in Japanese with English abstract)

————, Kawamura, M. and Kato, M. (1985) The Lower Carboniferous Odaira and Onimaru Formations in the Setamai-Yukisawa district, southern Kitakami Mountains, Northeast Japan. *Jour. Geol. Soc. Japan*, vol.91, p.851-866. (in Japanese with English abstract)

Kawano Y. and Ueda Y. (1965) K-Ar dating on the igneous rocks in Japan (II) : Granitic rocks in Kitakami Massif. *Sci. Rep. Tohoku Univ., Series III*, vol.9, p.199-125.

Kerrick, D.M. (1987) Fibrolite in contact aureoles of Donegal, Ireland. *Amer. Mineral.*, vol.72, p.240-254.

———— (1990) The $Al_2SiO_5$ polymorphs. *Rev. Mineral.*, vol.22, 406p., Mineralogical Society of America, Washington D.C.

———— and Speer, J.A. (1988) The role of minor element solid solution on the andalusite-sillimanite equilibrium in metapelites and paraluminous granitoid. *Amer. Jour. Sci.*, vol. 288, p.152-192.

Kobayashi, T. (1941) The Sakawa orogenic cycle and its bearing on the origin of the Japanese Islands. *Jour. Fac. Sci. Imp. Univ. Tokyo, sec.2*, vol.5, p. 219-578.

Kretz, R. (1983) Symbols for rock-forming minerals. *Amer. Mineral.*, vol.68, p. 277-279.

Labotka, T.C. (1981) Petrology of an andalusite-type regional metamorphic terrane, Panamint Mountains, California. *Jour. Petrol.*, vol.22, p261-296.

————, Papike, J.J. and Vaniman, D.T. (1981) Petrology of contact metamorphosed argillite from the Rove Formation, Gunflint Trail, Minnesota. *Amer. Mineral.*, vol.68, p.900-914.

Laird, J. (1988) Chlorites: Metamorphic petrology. In Baily, S.W. ed., *Hydrous phyllosilicates (exclusive of micas)., Rev. Mineral.*, vol.19, p.405-453.

Lepezin, G.G., Kuznetzova, I.K., Lavrent'ev, Yu.G. and Chemel'nicova, O.S. (1976) Optical methods of determination of the contents in cordierites. *Contrib. Mineral. Petrol.*, vol.58, p.319-329.

Myashiro, A. (1961) Evolution of metamorphic belt. *Jour. Petrol.* vol.2, p.277-311.

Montel, J.M., Marignac, C., Babey, P. and Pichavant, M. (1992) Thermobarometry and granite genesis: the Hercynian low-P, high-T anatectic dome (French Massif Central). *Jour. Metam. Geol.*, vol.10, p.1-15.

Morikiyo, T. (1984) Carbon isotopic study on coexisting calcite and graphite in the Ryoke metamorphic rocks, northern Kiso district, central Japan. *Contrib. Mineral. Petrol.*, vol.87, p.251-259.

————, Okuyama-Kusunose, Y., M. Ujiie, H. Tabata, T. Moriguchi, H., Sugai and K. Iwamasa (1989) Carbon

isotopic study on the limestone from the Tono contact metamorphic aureole. A comparison between the Tono and the Ryoke metamorphic rocks. *Abstr. 96 Ann. Meeting (Mito)*, Geol. Soc. Japan, p.600. (in Japanese)

———, Okuyama-Kusunose, Y., H, Tabata, T. Moriguchi, H. Sugai, K. Iwamasa and M. Ujiie (1992) $^{13}C$ enriched limestones from the Tono district, Kitakami Mountains, northern Japan. *Earth Science (Chikyu Kagaku)*, vol. 46, p.21-28. (in Japanese with English abstract)

Newton, R.C. and Haselton, H.T. (1981) Thermodynamics of garnet-plagioclase-$Al_2SiO_5$-quartz geothermometer. In Newton, R.C., Navrotsky, A. and Wood, J.B. eds. *Thermodynamics of minerals and melts*, Springer, p. 129-145.

Ohmoto, H. and Kerrick, D.M. (1977) Devolatilization equilibria in graphitic system. *Amer. Jour. Sci.*, vol.277, p.1031-1044.

——— and Poulson, S.R. (1989) Devolatilization equilibria in graphite-pyrite-pyrrhotite bearing pelites with application to magma-pelite interaction. *Contrib. Mineral. petrol.*, vol.101, p. 418-425.

Oho, Y. (1981) Slaty cleavage in Ojika Peninsula, South Kitakami Mountains. *Jour. Geol. Soc. Japan*, vol.87, p.657-673.

Okuyama, Y. (1980) Low-grade metapelites in the contact aureole around the Tono granodiorite pluton, Miyamori-Ohazama district, Kitakami Mountains. *Jour. Japan. Assoc. Mineral. Petrol. Econ. Geol.*, vol.75, p.359-371. (in Japanese with English abstract)

Okuyama-Kusunose, Y. (1985) Margarite-paragonite-muscovite assemblages from the low-grade metapelites of the Tono metamorphic aureole, Kitakami Mountains, Northeast Japan. *Jour. Japan. Assoc. Mineral. Petrol. Econ. Geol.*, vol.80, p.515-525.

——— (1988) Petrology of pelitic metamorphic rocks in the contact aureole around the Tono granodioritic mass, Kitakami Mountains, Northeast Japan. Ph. D. thesis, Tohoku University, Sendai.

——— Phase relations in andalusite-sillimanite type Fe-rich metapelites; Tono contact aureole, Japan. *Jour. Metam. Geol.* (in press.)

——— and Itaya, T. (1987) Metamorphism of carbonaceous material in the Tono contact aureole, Kitakami Mountains, Japan. *Jour. Metam. Geol.*, vol.5, p. 121-139.

———, Uruno, K. and Kitakami River-Sand Research Group (1991) Staurolite-bearing hornfels from the Tono contact metamorphic aureole, Kitakami Mountains. *Abstr. 98 Ann. Meeting (Matsuyama)*, Geol. Soc. Japan, p.245. (in Japanese)

Ozawa, K. (1984) Geology of the Miyamori Ultramafic complex in the Kitakami Mountains, northeast Japan. *Jour. Geol. Soc. Japan*, vol.90, p.697-716.

——— (1988) Ultramafic tectonite of the Miyamori ophiolite complex in the Kitakami Mountains, Northeast Japan: hydrous upper mantle in an island arc. *Contrib. Mineral. Petrol.*, vol.99, p.159-175.

———, Shibata, K. & Uchiumi, S. (1988) K-Ar ages of hornblende in gabbroic rocks from the Miyamori ultramafic complex, Kitakami Mountains. *Jour. Mineral. Petrol. Econ. Geol.*, vol.83, p. 150-159 (in Japanese with English abstract).

Pattison, D.R.M. (1989) P-T conditions and the influence of graphite on pelitic phase relations in the Ballachulish aureole, Scotland. *Jour. Petrol.*, vol.30, p.1219-1244.

——— and Tracy, R.J. (1991) Phase equilibria and thermobarometry of metapelites. in Kerrick, D.M., ed. *Contact metamorphism, Reviews in Mineralogy*, Vol. 26, Mineral. Soc. Amer.

Washington DC., p.105-206.

Pitcher, W.S. and Berger, A.R. (1972) The geology of Donegal: a study of granite emplacement. Wiley and Sons, Interscience, New York, 435pp.

Powell, R. and Holland, T. (1990) Calculated mineral equilibria in the pelitic system, KFMASH ($K_2O$-FeO-MgO-$Al_2O_3$-$SiO_2$-$H_2O$). *Amer. Mineral.*, vol.75, p.367-380.

Raymer, A.P.S., Matthews, A. and Navon, O. (1984) Pressure-temperature conditions in the Wadi Kid metamorphic complex; implications for the pan-African event in SE Sinai. *Contrib. Mineral. Petrol.*, vol. 85, p.336-345.

Saito, Y. and Hashimoto, M. (1982) South Kitakami region: an allochthonous terrane in Japan. *Jour. Geophys. Res.*, vol.87, p.3691-3696.

Seki, Y. (1954) On chloritoid rocks in the Kitakami Median Zone, north-eastern Japan. *Sci. Rep. Saitama Univ., ser.B*, vol.1, p.223-263.

——— (1957) Petrological study of hornfelses in the central part of the Median Zone of the Kitakami Mountainland, Iwate Prefecture. *Sci. Rep. Saitama Univ., ser.B*, vol.2, p.307-361.

Spear, F.S. and Cheney, J.T. (1989) A petrogenetic grid for pelitic schists in the system $SiO_2$-$Al_2O_3$-FeO-MgO-$K_2O$-$H_2O$. *Contrib. Mineral. Petrol.*, vol. 101, p.149-164.

Symmes, G.H. and Ferry, J.M. (1992) The effect of whole-rock MnO content on the stability of garnet in pelitic schists during metamorphism. *Jour. Metam. Geol.*, vol.10, p.221-237.

Uruno, K, Ujiie, M. and Kitakami River-Sand Research Group (1986) The first occurrence of staurolite-bearing rock from Kitakami Mountains, by river-sand survey. *Abstr. 93 Ann. Meeting (Yamagata)*, Geol.Soc.Japan, p.259. (in Japanese).

Wang, G.F., Banno, S and Takeuchi, K. (1986) Reactions to define the biotite isograd in the Ryoke metamorphic belt, Kii Peninsula, Japan. *Contrib. Mineral. Petrol.*, vol. 93, p.9-17.

——— and Banno,S. (1987) Non-stoichiometry of interlayer cations in micas from low - to middle-grade metamorphic rocks in the Ryoke and the Sanbagawa belts, Japan. *Contrib. Mineral. Petrol.*, vol. 97, p. 313-319.

## 北上山地，遠野接触変成帯の紅柱石－珪線石型接触変成作用；鉄に富む泥質岩における変成反応と相関係

奥山（楠瀬）康子

### 要　旨

北上山地白亜紀花崗岩類の中で最大の岩体である遠野花崗閃緑岩は，周囲の古生層に著しい接触変成作用を及ぼした．接触変成帯には，主として変成された泥質岩と石灰質岩が分布し，接触帯の幅は最大7 kmに達する．泥質岩は全般に$Al_2O_3$に富み，MnOに乏しく（MnO/MnO+MgO+FeO<0.01），Mnを含まない泥質岩系（$K_2O$-FeO-MgO-$Al_2O_3$-$SiO_2$-$H_2O$系）に近似できる．FeO/（FeO+MgO）比については，大多数の泥質岩が中間的組成（0.5-0.6）を持つが，それに加えFeに富む岩型（ラテライト質泥質岩とよぶ）も分布している．こうした全岩帯組成を反映して泥質変成岩には紅柱石・珪線石が広く含まれるほか，ラテライト質泥質岩を中心にクロリトイドを含む特徴的な鉱物組み合わせが認められる．中間組成の泥質岩とラテライト質泥質岩のそれぞれについ

て，石英・白雲母（高温ではカリ長石）と共存する鉱物組み合わせの系統的変化を追跡した．その結果から，接触変成帯を低温側から高温側へソーダ雲母帯・紅柱石帯・珪線石帯の三帯に分帯し，さらに各帯を下部・上部二つずつの亜帯に分けた．

中間組成の泥質岩は，ソーダ雲母帯ではソーダ雲母＋緑泥石＋白雲母（＋曹長石）の組み合わせを持つ．温度上昇にともなって次の順で鉱物の生成・消失が起こる；ソーダ雲母消失／紅柱生成，黒雲母生成，緑泥石消失／菫青石生成，白雲母消失／カリ長石生成，紅柱石－珪線石転移，アルマンディン生成．紅柱石帯および珪線石帯は，紅柱石の生成と，その珪線石への転移によって定義した．また，緑泥石消失／菫青石生成により紅柱石帯が，アルマンディン生成により珪線石帯が，それぞれ上部・下部亜帯に分帯される．

ラテライト質泥質岩は，ソーダ雲母帯の低温部でソーダ雲母＋緑泥石＋パイロフィライト組み合わせを持つ．パイロフィライトと緑泥石は，温度上昇とともに反応して，クロリトイドを生成する．クロリトイド生成により，ソーダ雲母帯は上部・下部亜帯に分けられる．クロリトイドは下部紅柱石帯においても安定で，紅柱石，黒雲母と共存する．クロリトイドは中間組成の泥質岩での菫青石生成に先だって消失し，上部紅柱石帯のラテライト質泥質岩では紅柱石＋黒雲母の組み合わせが安定となる．白雲母の安定なゾーンではアルマンディンは認められず，また，十字石も白雲母を欠く$K_2O$の乏しい岩型に限られる．

以上のような泥質岩鉱物共生には，次のような特徴がある．1）泥質岩全岩組成が$Al_2O_3$に富むため，ソーダ雲母が広く産出し，温度上昇とともに紅柱石に分解している．これは，ソーダ雲母が低圧の紅柱石領域で直接$Al_2SiO_5$鉱物を生成する関係を実証するものであり，世界的にみても希な産状である．2）ラテライト質泥岩にはクロリトイドが多産するが，白雲母の安定領域内ではより高温のゾーンにあってもアルマンディンが認められない．この関係は，Mnを含まない系では低温ではクロリトイドがアルマンディンに対して安定であるという理論的な予測（Symmes and Ferry, 1992）を支持する．3）低圧中間群および中圧型の泥質変成岩では，クロリトイドの累進的反応生成物として十字石が生成するが，遠野接触帯ではクロリトイドは直接黒雲母＋紅柱石組み合わせを生じている．こうした累進的反応関係は，典型的な低圧変成作用を特徴づける可能性がある．

接触帯の変成条件を，炭素同位帯温度計，ざくろ石－黒雲母温度計，ざくろ石－斜長石－石英－$Al_2SiO_5$圧力計と，白雲母＋石英およびソーダ雲母＋石英の脱水反応を組み合わせて求めた．変成作用の温度は，ソーダ雲母帯約490°C以下，紅柱石帯490～600°C，下部珪線石帯600～670°C，上部珪線石帯670～730°C，圧力は約2.3 kbarと推定した．

（受付：1993年1月14日；受理：1993年5月24日）

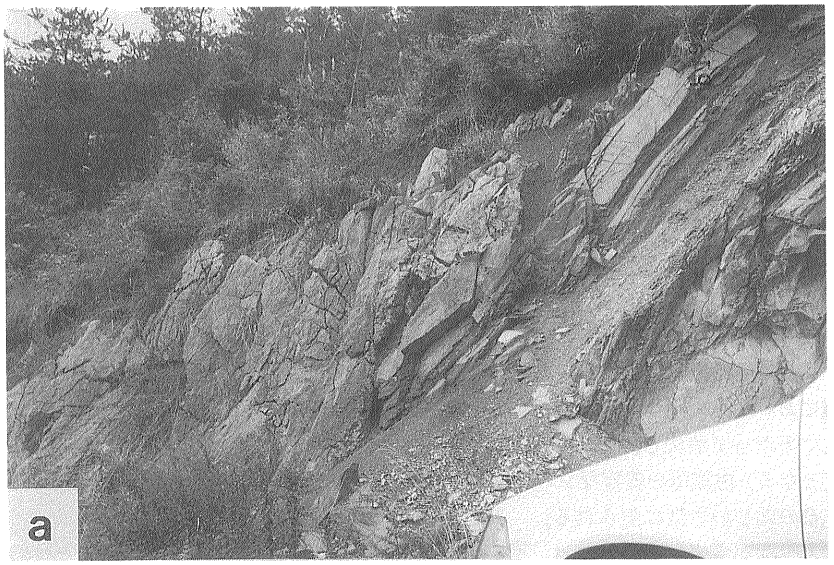


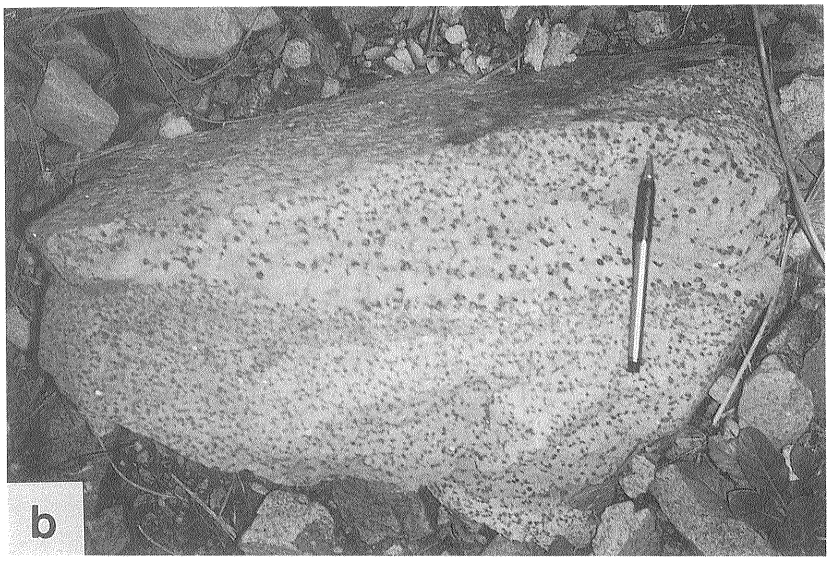


Plate I

a. An outcrop of chloritoid-bearing metapelite (upper paragonite subzone). The chloritoid-bearing metapelite is intercalated with grey-colored limestone of Lower Carboniferous (equivalent to Odaira Formation). Aryunai Path (about 0.3km north of the locality of sample Nak-154).

b. Large idioblasts of chloritoid in the lower andalusite subzone. Shittakazawa (at the locality of Shi-11b).

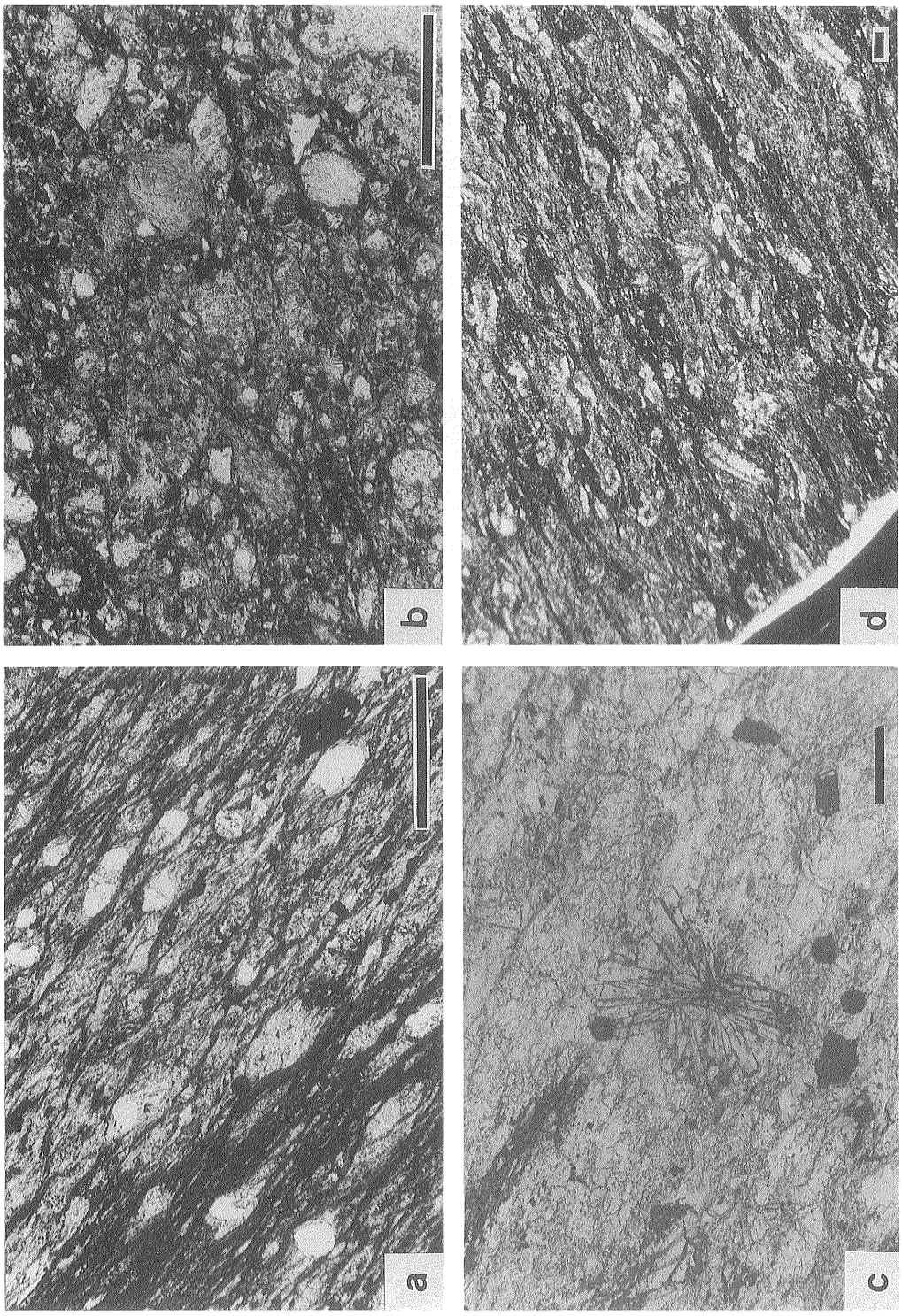


Plate II

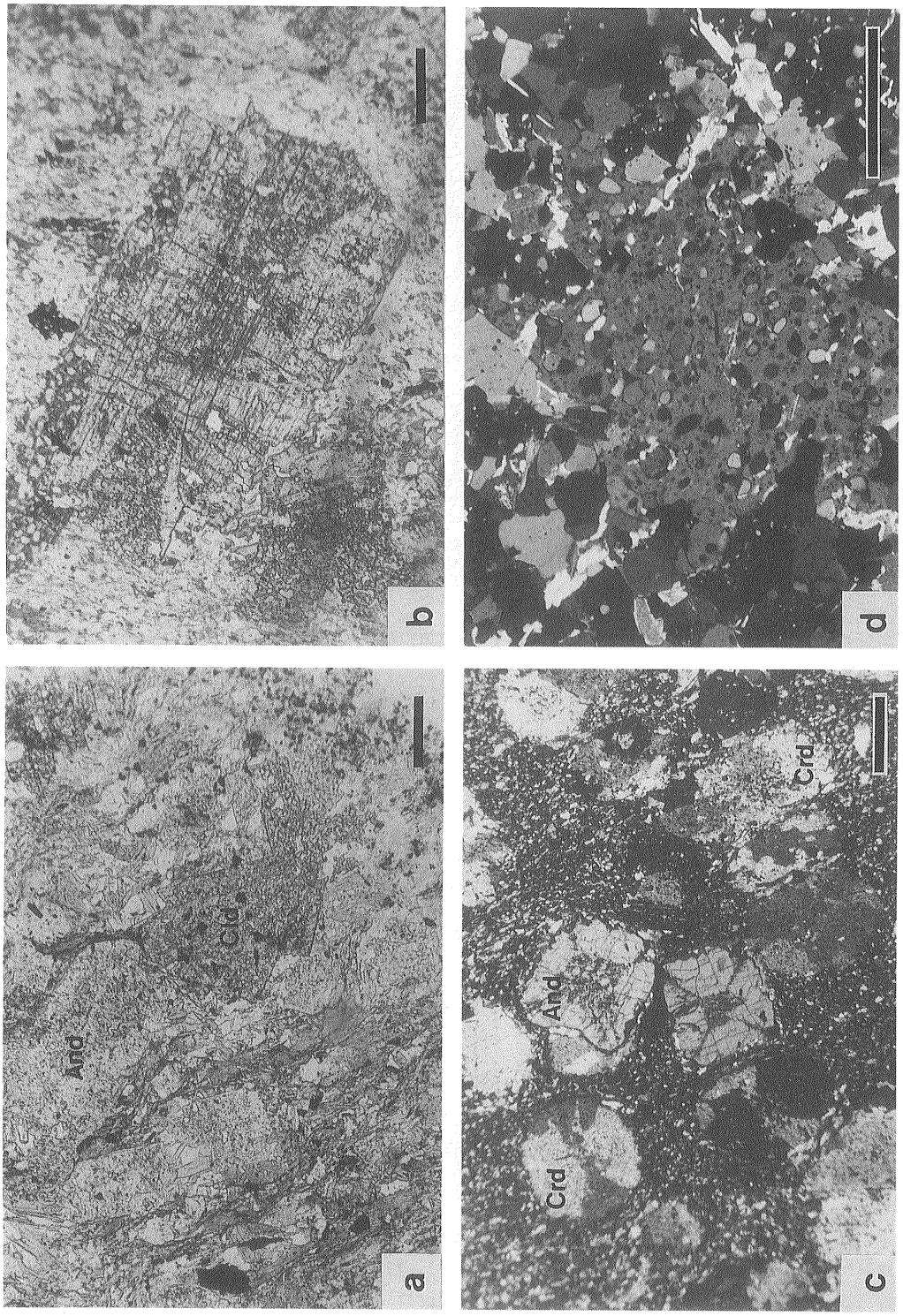


Plate III

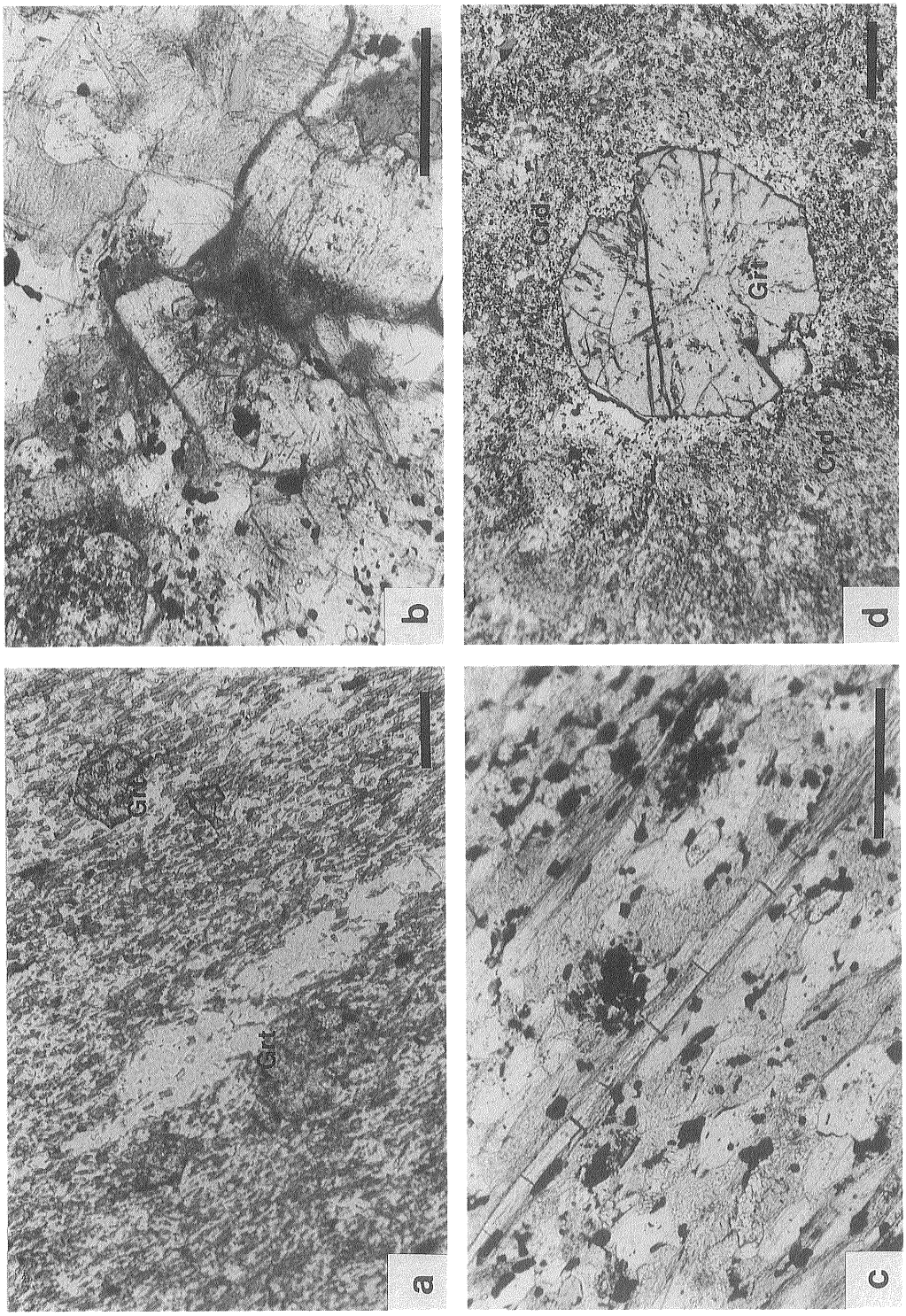


Plate IV

Plate II Photomicrographs of metapelite in the paragonite zone and lower andalusite subzone. Scale bar = 0.2mm

a. Texture of pelitic slate in the lower paragonite subzone. Dark-colored streaks run subparallel with each other intercalating lensoid aggregates of micas and chlorite. Sample 906-01. Plane polarized light.
b. Textures of metapelite in the upper paragonite subzone. Slaty texture becomes indistinct due to overall grain coarsening. Sample Nak-154. Plane polarized light.
c. Chloritoid "rosette" in the upper paragonite subzone. Sample 509-04. Plane polarized light.
d. Minute grains of andalusite occurring near the andalusite isograd. Sample Man-40. Plane polarized light.

Plate III Photomicrographs of metapelites in the lower and upper subzones of the andalusite zone.

a. Andalusite (And) and chloritoid (Cld) coexisting in a lateritic metapelite containing biotite, muscovite and quartz. Sample 509-07 (lower andalusite subzone). Plane polarized light. Scale bar = 0.2mm.
b. A large idioblast of chloritoid in the sample Shi-11b (lower andalusite subzone). The grain shows distinct hourglass structure. Plane polarized light. Scale bar = 1 mm.
c. Euhedral andalusite (And) showing chiastolitic inclusion pattern and rounded cordierite (Crd) in a pelitic hornfels of the upper andalusite subzone. Cordierite is relatively poor in inclusions, and frequently forms characteristic penetrative twin. Sample 614-21. Cross-polarized light. Scale bar = 0.5mm.
d. Irregularly shaped cordierite in coexisting with K-feldspar (upper andalusite subzone). Cordierite includes abundant grains of quartz and micas. Sample 616-04. Cross-polarized light. Scale bar = 0.2mm.

Plate IV Photomicrographs of metapelites in the high-grade zones.

a. Small grains of almandine garnet (Grt) in fine-grained matrix composed of biotite, quartz, andesine and K-feldspar. Sample Shr-64 (upper andalusite subzone). Plane polarized light. Scale bar = 0.2mm.
b. Fibrolite mat surrounding relic andalusite in Sample Wak-135 (lower sillimanite subzone). Plane polarized light. Scale bar = 0.5mm.
c. Elongated sillimanite prisms running parallel with each other. Sample Kum-15 (lower sillimanite subzone). Plane polarized light. Scale bar = 0.2mm.
d. Euhedral garnet (Grt) coexisting with cordierite (Crd) and brown biotite. Sample Ft-19 (upper sillimanite subzone). Plane polarized light. Scale bar = 0.5mm.